AGU PUBLICATIONS

JGR

Journal of Geophysical Research: Oceans

RESEARCH ARTICLE

10.1002/2017JC013356

Acoustic Tomography in the Canary Basin: Meddies and Tides

Brian D. Dushaw[1], Fabienne Gaillard[2], and Thierry Terre[2]

[1]Nansen Environmental and Remote Sensing Center, Bergen, Norway, [2]IFREMER, Univ. Brest, CNRS, IRD, Laboratoire d'Océanographie Physique et Spatiale, IUEM, Plouzané, France

Key Points:
- Meddies and stochastic parcels of Mediterranean water are important factors in understanding the acoustic forward problem
- The presence of Mediterranean water is observed by acoustic tomography to be variable and persistent
- Mode-1 internal tides observed in the Canary Basin are partly predicted using a global model derived from satellite altimetry

Correspondence to:
B. D. Dushaw,
brian.dushaw@nersc.no

Citation:
Dushaw, B. D., Gaillard, F., & Terre, T. (2017). Acoustic tomography in the Canary Basin: Meddies and tides. *Journal of Geophysical Research: Oceans*, *122*, 8983–9003. https://doi.org/10.1002/2017JC013356

Received 15 AUG 2017
Accepted 20 SEP 2017
Accepted article online 26 SEP 2017
Published online 22 NOV 2017

Abstract An acoustic propagation experiment over 308 km range conducted in the Canary Basin in 1997–1998 was used to assess the ability of ocean acoustic tomography to measure the flux of Mediterranean water and Meddies. Instruments on a mooring adjacent to the acoustic path measured the southwestward passage of a strong Meddy in temperature, salinity, and current. Over 9 months of transmissions, the acoustic arrival pattern was an initial broad stochastic pulse varying in duration by 250–500 ms, followed eight stable, identified-ray arrivals. Small-scale sound speed fluctuations from Mediterranean water parcels littered around the sound channel axis caused acoustic scattering. Internal waves contributed more modest acoustic scattering. Based on simulations, the main effect of a Meddy passing across the acoustic path is the formation of many early-arriving, near-axis rays, but these rays are thoroughly scattered by the small-scale Mediterranean-water fluctuations. A Meddy decreases the deep-turning ray travel times by 10–30 ms. The dominant acoustic signature of a Meddy is therefore the expansion of the width of the initial stochastic pulse. While this signature appears inseparable from the other effects of Mediterranean water in this region, the acoustic time series indicates the steady passage of Mediterranean water across the acoustic path. Tidal variations caused by the mode-1 internal tides were measured by the acoustic travel times. The observed internal tides were partly predicted using a recent global model for such tides derived from satellite altimetry.

Plain Language Summary Long-range acoustic transmissions in the Canary Basin between the Canary and Azores Islands are used to examine the ability of such acoustic signals to measure or determine properties of warm, salty Mediterranean water. Such water originates from the Mediterranean, and it advects or defuses into the subtropical Atlantic at about 1200 m depth through the Canary Basin. The water is often organized into compact rotating eddies. The effects on the acoustic propagation of this warm and salty water are considerable, but the exact nature of the water masses proved difficult to pin down by this means. The observations indicate a steady presence of Mediterranean water, however. Internal tides, the vertical displacement of water properties caused by the tides, were also observed, and this variability could be partly predicted by a global tidal model derived from satellite altimetry.

1. Introduction

Seawater flowing out of the Mediterranean through the Strait of Gibraltar is warmer and saltier than Atlantic water. This water has the same density as water at about 1,000–1,200 m depth in the eastern subtropical Atlantic; the temperature and salinity deviations from ambient values are density compensating. The volume of seawater flowing out of the Mediterranean is substantial, and it eventually forms a large water mass called Mediterranean water that extends across the subtropical North Atlantic at intermediate depths. Much of this water mass is transported by self-contained, rotating eddies, called salt lenses or Meddies, of 50–100 km horizontal extent and several hundred meters vertical extent (Richardson et al., 2000). Meddies move at a nominal speed of about 2–4 cm s^{-1} and circulate with speeds of about 20 cm s^{-1} (Richardson & Tychensky, 1998). Since Meddies are both deep and density compensated, they are difficult to detect and observe. Indeed, Meddies were first observed by chance in hydrographic casts (Armi & Zenk, 1984). One extraordinary development in recent years has been the use of seismic imaging to determine the detailed structures of Meddies and their surrounding environment (Biescas et al., 2008, 2014; Papenberg et al., 2010; Pinheiro et al., 2010; Quentel et al., 2011). Satellite altimetry has been used to locate and track Meddies (Bashmachnikov et al., 2009; Ienna et al., 2014; Stammer et al., 1991), although there are technical

challenges in identifying unique Meddy characteristics in sea-surface height and in overcoming the limited spatial resolution of satellite observations. An essential characteristic of the environment of the Canary Basin near the sound channel axis is the diffusion, advection, or propagation of Mediterranean water southwestward. Long standing issues are the net southwestward flux of this warm and salty water and the mechanisms for this flux (Richardson et al., 2000).

While Mediterranean water is density compensated, its warm and salty properties (T about 12°C, S about 36) make its sound speed considerably faster than ambient sound speed. Typical Meddy temperature anomalies are about 3°C and salinity anomalies are about 1 ppt, both of which make the speed of sound within Meddies about 12 m s^{-1} faster than surrounding waters. In the Canary Basin, a 1°C temperature variation corresponds to about 3.6 m s^{-1} sound speed variation, while a 1 ppt salinity variation corresponds to about 1 m s^{-1} sound speed variation. In addition, since this water type lies near the sound channel axis at 1,000–1,200 m in the eastern subtropical Atlantic, it could be expected to significantly affect near-axis acoustic propagation. These properties suggest that Mediterranean water may be observed using acoustical methods, and acoustic tomography, in particular. The application of tomography for observing Meddies has been examined by theory or simulation in the past (Mikhin et al., 1997; Voronovich & Shang, 1999), and the conclusions of those studies suggested a practical utility to such observations. Mikhin et al. (1997) examined the effects of Meddy currents on tomographic signals. These effects are expected to be small, however.

The "Canary-Azores-Madeira Basin Integral Observing System" (CAMBIOS) experiment was designed to test the ability of acoustic tomography to measure properties of Mediterranean water and its flux. CAMBIOS took place in the Canary Basin from July 1997 to April 1998 (Figure 1), as part of the European project "Canary Islands Azores Gibraltar Observations" (CANIGO; Parrilla et al., 2002). In order to measure integrated heat content and detect temperature anomalies (Figure 2), acoustic tomography transceivers spanning the Canary Basin were deployed for approximately 9 months. Simplistically, the experiment was designed to

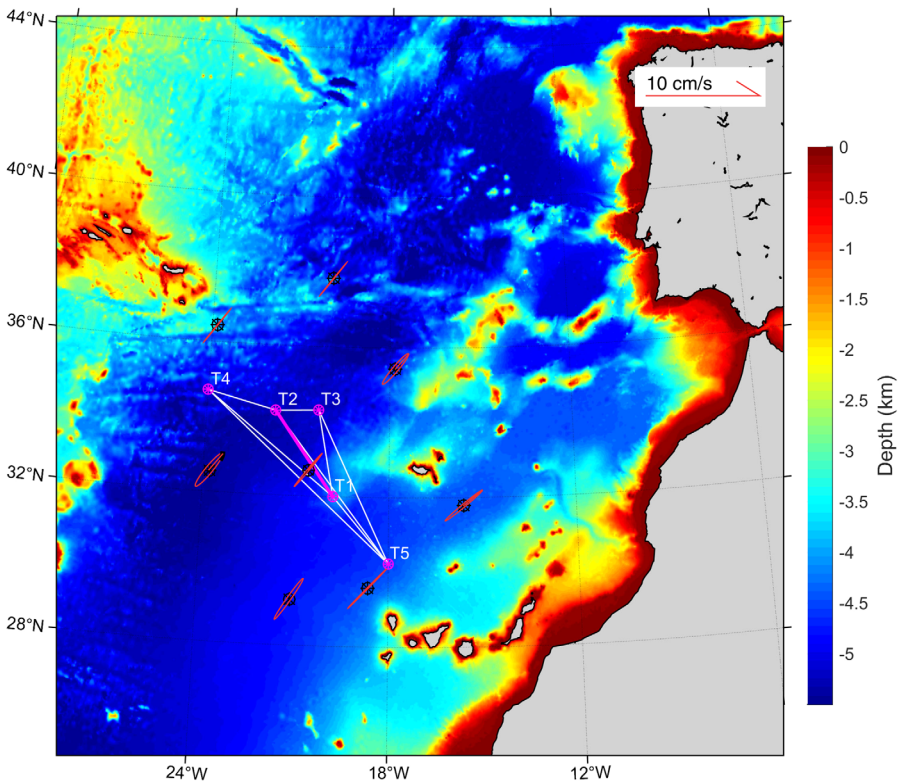

Figure 1. The CAMBIOS array was located across the Canary Basin and oriented so as to observe the southwestward flux of Mediterranean water. The Canary Basin is the primary avenue for movement of Mediterranean water into the western Atlantic. The M_2 tidal current elipses, denoted in red, were derived from the TPXO tidal model. The T1–T2 acoustic path was along the small minor axis of tidal current, hence the observed signal from tidal currents was small. Azimuthal equal area projection.

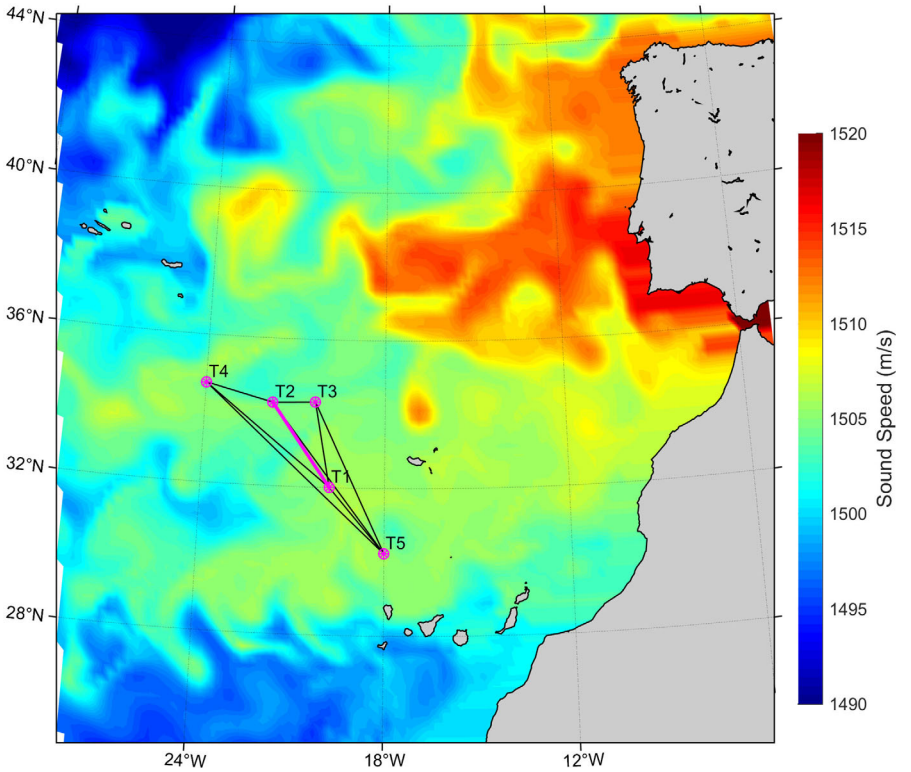

Figure 2. The CAMBIOS observing array and sound speed at 1,000 m depth on yearday 192, 2004 derived from the Estimating the Circulation and Climate of the Ocean, Phase II (ECCO2) project ocean state estimates (Dushaw et al., 2013; Menemenlis et al., 2008). ECCO2 was a global numerical model for the temporal evolution of ocean temperature, salinity, currents, etc. at 1/4° resolution fit to a wide range of available ocean data and forcing using data assimilation. Warm, salty water from the Mediterranean makes its way into the western subtropical Atlantic through the Canary Basin.

count Meddies. The previous year, also as part of CANIGO, but not part of CAMBIOS, tomography had been employed within the Strait of Gibraltar as a way to obtain integral measurements of mass and heat transports through the Strait itself (Send et al., 2002; Tiemann et al., 2001). The entire CAMBIOS data set is publicly available.

For this paper, our limited purpose is a description of the acoustic forward problem for the acoustic data obtained during the CAMBIOS experiment, drawing on the available measurements in support of that purpose. Understanding the nature of the observed arrival patterns is an essential part of the process of developing procedures to estimate temperature variations by inversion of the acoustic data (Dushaw et al., 2016); this is the forward problem of ocean acoustic tomography (Cornuelle et al., 1993; Munk et al., 1995). The main results of the present paper are therefore a description of the CAMBIOS tomography experiment and a discussion of the nature of the acoustic propagation of the region. The nature of the measured arrivals suggests vigorous acoustic scattering is occurring, as is commonly observed near the finale of midlatitude arrival patterns, e.g., Colosi et al. (2005). We conclude that the Mediterranean water influences acoustic propagation in a variety of ways, by parcels of warm, salty water stochastically distributed along the sound channel axis and by coherent Meddies. The goal of the analysis was to obtain a detailed understanding of the acoustic propagation such that inverse methods could be devised to determine properties of Meddies or Mediterranean water from the acoustic data.

In sections 2 and 3, the CAMBIOS tomography program and associated acoustic, moored, and hydrographic data are described. In section 4, a computed acoustic arrival pattern is compared to the observations for an identification of the ray arrivals. In section 5, models for small-scale, stochastic variations in sound speed caused by internal waves and spice variations are employed to account for aspects of the acoustic arrival patterns. In section 6, a simple model for a Meddy is employed to illustrate the main travel time and arrival pattern signals of such a feature, as it would be observed by acoustic tomography. In section 7, the effects

of horizontal refraction of the acoustic propagation by a Meddy are shown to be inconsequential. In section 8, the barotropic and internal tide variations observed by the acoustic travel times are compared to predictions by global tidal models. Finally in section 9, the analysis is briefly summarized and discussed.

2. CAMBIOS Tomography

The CAMBIOS acoustic array consisted of five moorings denoted T1–T5 deployed across the Canary Basin between the Canary and Azores Islands (Figure 1; Gaillard & Terre, 2003, 2004; Terre & Gaillard, 2003). Because of a number of instrument failures, acoustic data were mainly obtained between the T1 and T2 moorings. The T1 mooring was located at 31.9988°N, 19.8008°W in about 4,150 m ocean depth, and the T2 mooring was located to the northwest at 34.2473°N, 21.75002°W in about 5,275 m ocean depth (Figure 1). The acoustic propagation was over 308.692 km range over the smooth Madeira Abyssal Plain. In addition, the acoustic path was across the Azores Current (Fründt & Waniek, 2012), characterized by 1–3°C changes in temperature down to about 1,000 m depth. The acoustic sources, moored at 660 and 700 m depths, made reciprocal transmissions for 265 days, beginning on yearday 190 in June 1997 and ending on yearday 454 in early April 1998. The signals were received at the receiving mooring by two hydrophone subarrays located just above each source. The T1 source transmitted 3,102 times, while the T2 source transmitted 3,166 times. The reciprocal transmissions were not precisely simultaneous, but separated by 20 min.

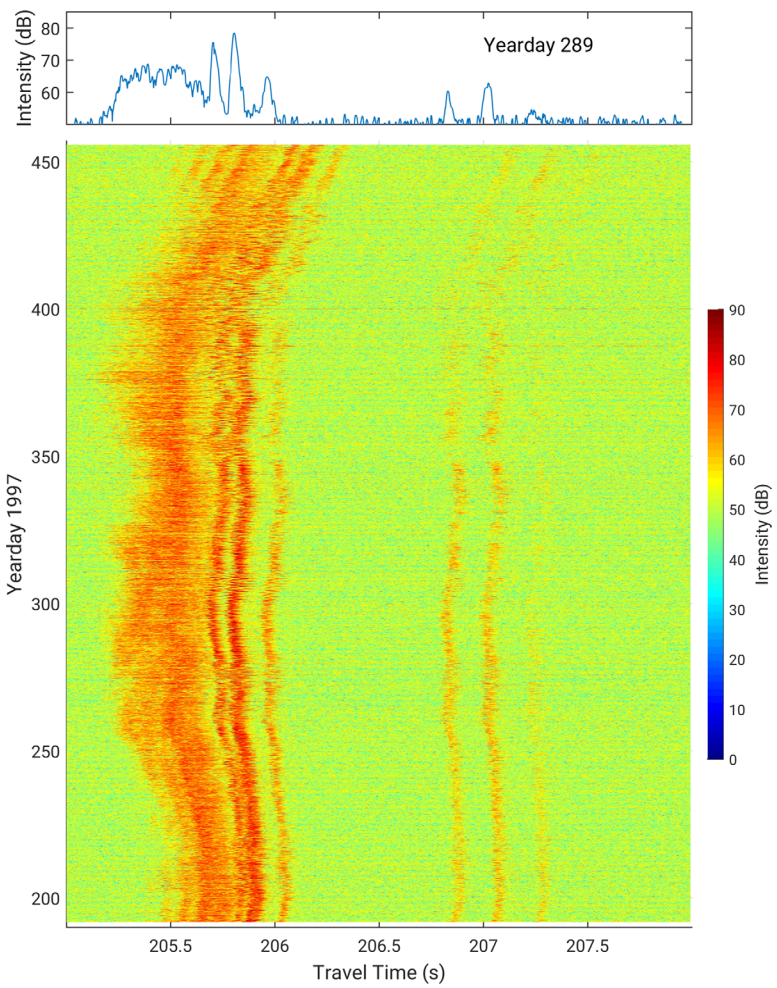

Figure 3. Acoustic receptions obtained along the T1–T2 acoustic path. The profile of a reception on yearday 289 is given in the top. About seven stable ray arrivals are evident, including a doublet arrival that appears in the top the largest amplitude peak and the three late-arriving bottom-reflected rays.

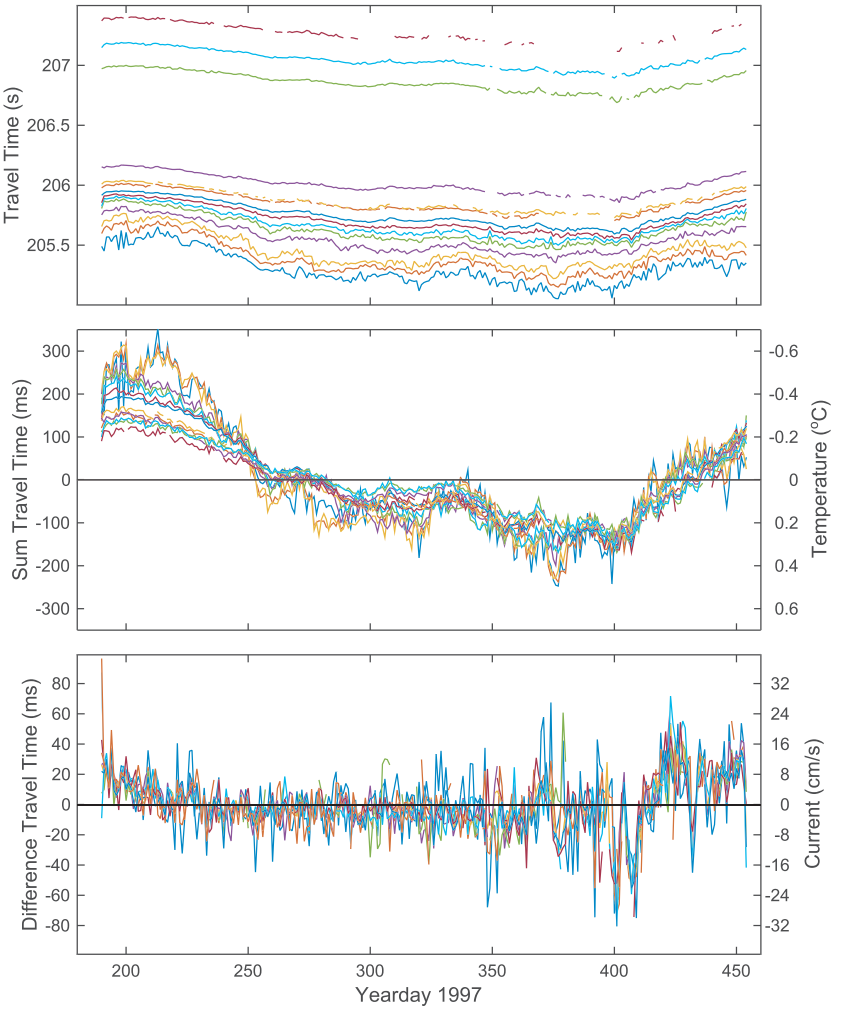

Figure 4. Tracked ray travel times. (top) The average of reciprocal travel times. The three late arrivals are bottom reflections, or RBR, rays. (middle) Travel times with the mean travel times removed to better show the temperature variations. An approximate temperature scale for depth-average and range-average temperature is given at right. (bottom) The difference of reciprocal travel times indicating ocean current. An approximate current scale for depth-average and range-average current is given at right. Positive current is southwestward.

The acoustic sources, obtained from Webb Research Corporation (now Teledyne Webb Research), operated at a source level of 180 dB Re 1 μPa @ 1 m at 400 Hz center frequency with 100 Hz bandwidth (Spindel et al., 1982). The "organ pipe" sources were deployed with sufficient energy for 160 h of transmisions. The transmissions consisted of 511-digit maximal length shift register sequences, with each digit lasting four carrier cycles, or 10 ms. The total sequence duration was 5.11 s. Transmissions consisted of a set of three patterns of 16 and 31 sequences at 2 h intervals for the 275 day duration of the experiment (Terre & Gaillard, 2003). The transmission schedule was partly designed to allow tidal signals to be filtered. After recovery, the recorded signals were processed by pulse compression techniques to form the equivalent impulse response signal. After pulse compression, the transmitted signals offered a time resolution of 10 ms. The range between the two moorings was limited to 300 km to allow for adequate received signal-to-noise ratio.

The receiving arrays on each mooring consisted of two subarrays of four hydrophones, each comprising a receiver channel. That is, each of the two channels provided data from the combined signals of four hydrophones by hardware design. The four hydrophones on each subarray were spaced by a half wavelength with three points of measurement in a 1–2-1 weighting. The center point consisted of two of the hydrophones hardwired together. The subarrays were spaced by a half wavelengths, or about 1.875 m, so they overlapped by a half wavelength. While these two data channels could in principle be combined by beamforming

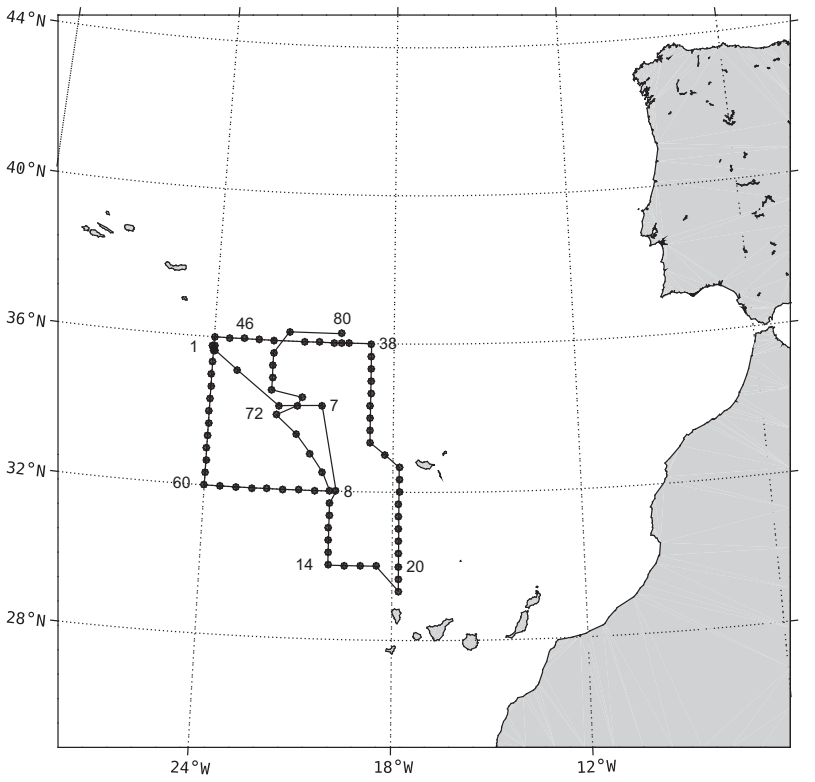

Figure 5. Positions of 80 CTD casts obtained during CAMBIOS deployment in summer 1997.

techniques to provide a crude determination of ray arrival angle, for unknown reasons the first channel had significantly less signal and greater noise than the second channel. For this reason, only data from channel 2 are employed here, without beamforming. In processing these data, a beamforming capability would

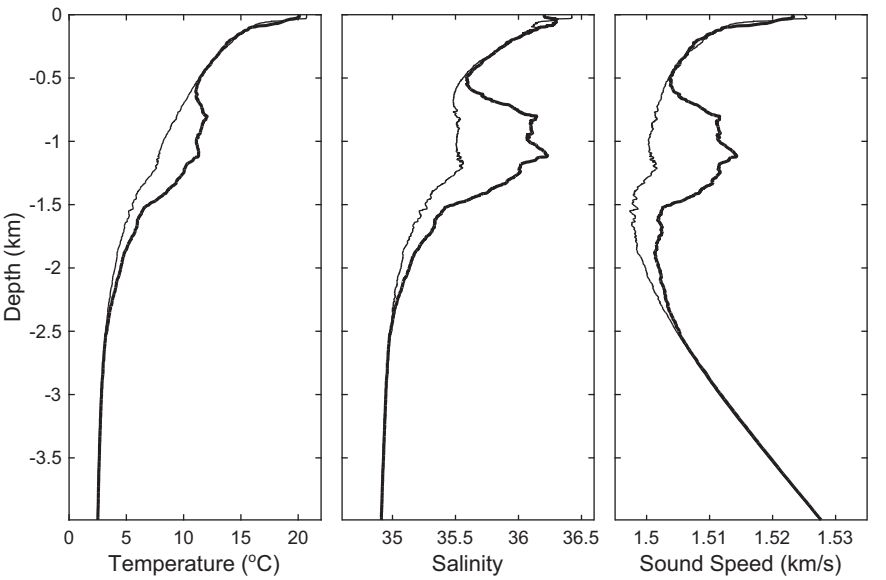

Figure 6. Temperature, salinity, and sound speed derived from nearby CTD casts obtained during the deployment of CAMBIOS moorings. A Meddy (thick line) was observed at 35.7597°N, 23.9429°W, while a CTD cast about 150 km away (thin line) at 34.2499°N, 21.7502°W measured no Meddy signature. The Meddy had temperatures about 3°C warmer, salinities about 0.6 ppt greater, and sound speeds 10–14 m s^{-1} faster than ambient water.

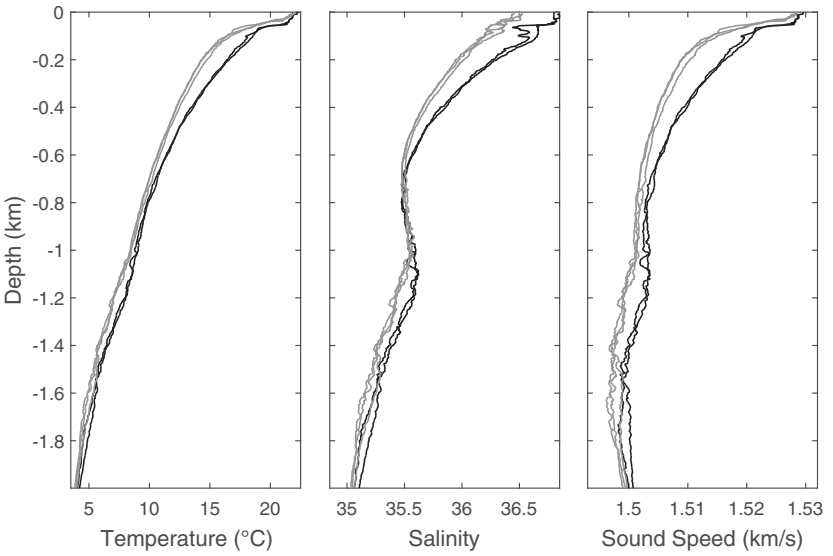

Figure 7. Five profiles of (left) temperature, (middle) salinity, and (right) sound speed obtained from CTD casts along the CAMBIOS T1–T2 tomography path during the deployment cruise. The path crossed the Azores Current which separates Western (18°C, black lines) from Eastern (15°C, gray lines) Atlantic water.

obviously have been advantageous, particularly in distinguishing coinciding doublet ray arrivals with opposite angles.

The travel times were corrected for the motion of the source and receiver moorings (Gaillard et al., 2006). The instrument clock times were checked at deployment and recovery, but time keeping during the experiment relied on temperature compensated quartz oscillators. Clock errors affecting measurements of currents at low frequencies are therefore possible from the clock frequency errors. Sound speed was measured using the sum of reciprocal travel times which removes clock error. After the processing and corrections, the recorded travel time of any given pulse could be determined to about 10 ms precision, assuming the cancellation of clock error.

A second acoustic source, deployed on the T5 mooring 5 months after the start of the experiment, had been designed and constructed by IFREMER with 400 Hz center frequency and 50 Hz bandwidth. This acoustic source produced a sound level of 195 dB Re 1 μPa @ 1 m, but it failed after just two transmissions as a result of a leak through an electrical connector into the battery container (Gac et al., 1998, 1999). This source was subsequently lost during recovery operations when a cable failed in rough seas. The receiving hydrophones on moorings T3 and T4 failed less than 2 days after deployment because of a failed connector. As a result, complete time series of travel times were obtained only along the T1–T2 acoustic path.

3. Data Description

3.1. Tomography Data

The recorded arrival pattern was mostly stable and consistent over the entire experiment (Figure 3). The reception begins with a scattered or stochastic section of about 0.5 s duration, followed by a small set of stable ray arrivals, and ending with three delayed arrivals. The pattern of stable ray arrivals is consistent with patterns predicted using the 2009 World Ocean Atlas (WOA09; Antonov et al., 2010; Del Grosso, 1974; Locarnini et al., 2010), as described further below. These patterns were readily tracked to form time series of ray travel times (Figure 4). The overall arrival pattern is reversed from the usual pattern at midlatitudes in the world's oceans in that the small-angle, near-axis rays arrive first. For this reason, we term the initial stochastic section of the arrival pattern the "overture," in parallel with the use of the term "finale" for those patterns in which near-axis acoustic energy arrives last. The pattern is likely governed by the local increase in sound speed near the sound channel axis as a consequence of Mediterranean water. Alternatively, there are two sound speed minima straddling the sound channel axis, but these minima are not usually sufficient to separately trap acoustic energy.

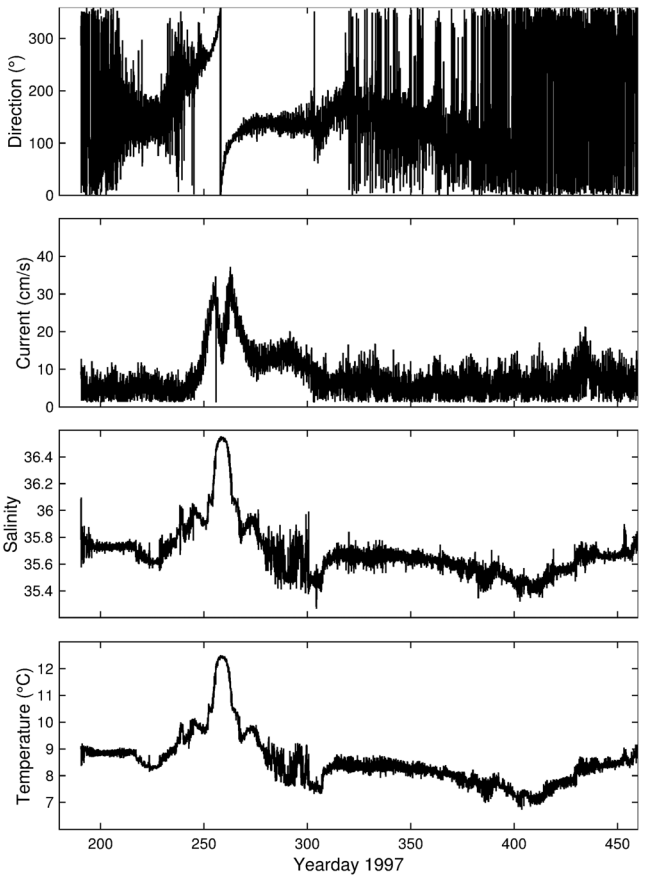

Figure 8. From bottom to top, time series of temperature, salinity, current speed, and current direction obtained on the T3 mooring located at 34.2985°N, 20.3317°W. The temperature and salinity measurements were at 1,200 m depth, while the current measurements were at 1,000 m depth.

Over the course of the 265 day record length the time series of recorded arrivals varied in travel time by about 300 ms, as shown in the sum of reciprocal travel times (Figure 4), mainly in a low-frequency variation resembling an annual cycle. Travel times are smallest, corresponding to the warmest water, around January 1998, however, the opposite of what might be expected from a seasonal cycle. In addition, these variations affected all acoustic rays similarly. Since, as will be shown below, some rays had upper turning points below about 500 m depth, observed temperature variations were unrelated to local surface forcing. Obvious oceanographic variations caused by mesoscale variations occurred at weekly to monthly time scales with variations of about 50 ms affecting all ray travel times about equally.

The difference of reciprocal travel times (Figure 4), exhibited a large positive trend, arising from clock error. This trend was removed by fitting a line to the differential travel time data, and subtracting that linear trend. The differential travel times changed by a large 2.5 ms/d. Clock drift is, of course, not necessarily linear, so remaining low-frequency variations in differential travel time may be a result of such error.

Figure 4 indicates rough estimates of temperature and current variability that correspond to the travel time variations.

3.2. Hydrography

Eighty conductivity-temperature-depth (CTD) casts were obtained during deployment cruise (Figure 5), and 69 casts were obtained during the recovery cruise (Gaillard et al., 1998, 1999a, 2015). Ninety-eight type T-5 XBT casts to 1,800 m depth were obtained during recovery. Neither the recovery CTD nor XBT data were employed for this analysis, however. Fortuitously, the first CTD cast north of mooring T4 during the deployment cruise observed the characteristic temperature and salinity anomalies of a Meddy (Figure 6). Compared to later CTD casts, 150 km distant, the Meddy had temperature anomalies of $+3$°C and salinity anomalies of $+0.6$ ppt. The Meddy sound speed anomalies were therefore $+10$ to 14 m s^{-1}.

While the CTD casts constituted a hydrographic survey of the Canary Basin region, the five casts 68–72 were obtained along the T1–T2 tomography path during the deployment cruise with about 77 km spacing (Figure 7). The first two of these casts were south of the Azores Current, while the last three of these casts were north of the Current, as shown by the distinct temperature and salinity properties on either side of the Current. The sound speed change as the Current is crossed is almost 10 m s^{-1} and the influence of the differing water masses extends to almost 2,000 m depth. These casts show the fluctuations in water properties caused by Mediterranean water parcels at 1,000–1,500 m depths. In addition, two sound speed minima at about 1,000 and 1,700 m are evident.

3.3. Moored Thermistors and Current Meters

Each of the T1–T4 moorings included thermistors at 500, 700, 1,000, 1,200, and 3,500 m depths (Gaillard et al., 1999b). A SEACAT was employed for the measurements at 1,200 m depth which also included salinity. Aanderaa RCM8 rotor current meters were deployed on each mooring at 500, 1,000, and 3,500 m depths. Near the sound channel axis at about 1,200 m, the variations in temperature were episodic with shifts in temperature of about 1°C occurring at irregular intervals.

At mooring T3, the clear signatures of a Meddy were observed by temperature, salinity, and current records. These measurements captured a nearly complete cross section of a Meddy as it passed the mooring around yearday 260 (Figure 8), as indicated by the minimum in current speed and the reversal of current direction. The Meddy carried water that was almost 4°C warmer than ambient water and salinity that was almost 1 ppt saltier, corresponding to a sound speed anomaly of about 17 m s^{-1}. The Meddy traversed the mooring in about 30 days, but the total Meddy event, including leading and trailing effects, lasted about 60 days. Meddies circulate in a clockwise direction when viewed from above. With an initial current direction of

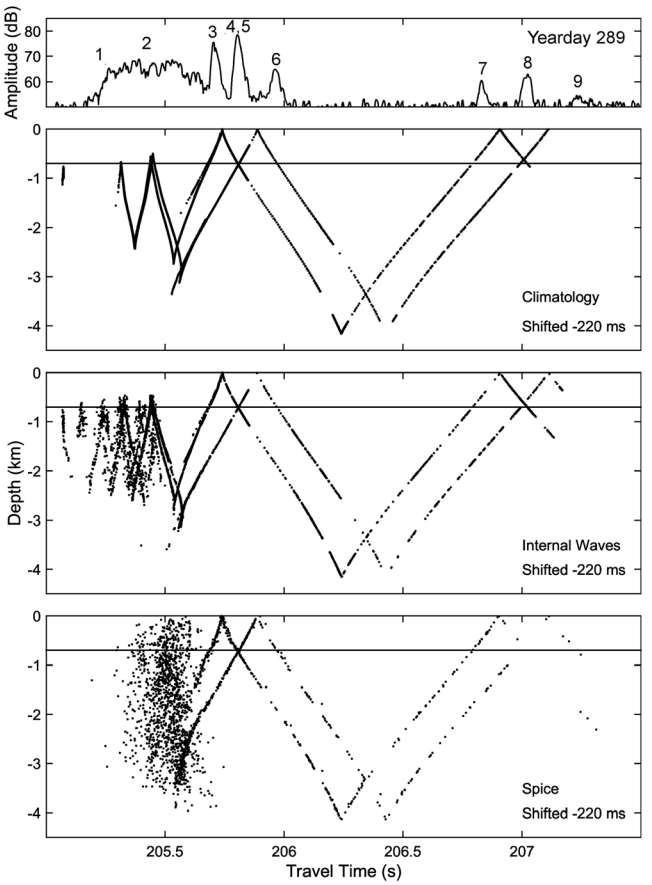

Figure 9. (top) Average arrival pattern for acoustic data obtained on yearday 289, 1997. Nine rays were tracked, as indicated. (top middle) Timefront for WOA09. (bottom middle) Timefront for WOA09 plus a single realization for internal waves. (bottom) Timefront for WOA09 plus spice.

250°–300° (relative to North) followed by a current direction of 90°–120°, these data are consistent with a relatively strong Meddy moving southwestward. Indeed, the movement of Meddies in the Canary Basin is reliably to the southwest (Richardson et al., 2000; Richardson & Tychensky, 1998), and this event would have taken about 30 days to reach the T1–T2 acoustic path.

4. Ray Tracing Predictions and Ray Identification

Using any given sound speed section, it is a simple matter to trace rays through it to obtain predictions for the acoustic arrival patterns for any source and receiver combination (Cornuelle et al., 1993; Dushaw & Colosi, 1998; Dushaw et al., 2013; Jensen et al., 1994; Munk et al., 1995). Acoustic tomography usually relies on the resolution of individual ray arrivals, and stable ray arrivals were evident in the data obtained (Figures 3 and 4). The arrivals of acoustic rays are typically evident as a sequential pattern of clear, narrow peaks of acoustic energy, repeated over the entire record. Once a computed arrival pattern is correlated with a measured arrival pattern, the ray arrivals are identifiable. This identification determines the spatial sampling associated with each ray arrival.

Acoustic propagation along the T1–T2 path over the Madeira Abyssal Plain was bottom limited to around 4,000 m. On this section the depth varied only gradually. We employed the Smith-Sandwell global topographic database version 12.1 (Smith & Sandwell, 1997). The bottom topography of the region consists of a flat abyssal plain, ideally suited for well-behaved bottom reflections.

The timefront (the arrival pattern at a given range as a function of travel time and arrival depth) was computed using a sound speed section computed from WOA09 (Figure 9). The arrivals in the timefront at the depth of the CAMBIOS receiver can be aligned to the observations. This alignment, requiring an advance in the predicted travel time of 220 ms (the climatology had a cold bias), shows that ray arrivals following the overture can be readily identified. In Figure 9, four clear ray arrivals between 205.6 and 206 s are evident, although in the observations two are superimposed. These are deep-turning rays, with arrival angles about 10°, lower turning depths around 3,500 m, and upper turning depths near or at the surface. In addition, there are three late arriving rays around travel time 207 s. These late arriving pulses corresponded to rays that had reflected from the seafloor near mooring T1 1–3 times. In both of these ray groups, coincident rays of opposite ray angle are evident. Such ray arrivals were indistinguishable in the data, given the inability to estimate ray angle. The required 220 ms shift in predicted travel times was not unusual; travel times varied by about 300 ms over the course of the 9 month record length (Figure 4). The ray identification process was repeated using sound speed profiles derived from the five CTD casts obtained during deployment along the acoustic path (Figure 7), with similar results, including the required travel time offset.

There are two obvious discrepancies between the predicted and measured patterns. First, the predictions from climatology obtain almost no acoustic energy consistent with the broad, stochastic overture that extends from about 205.25 to 205.6 s. Second, the weak last arrival at about 207.25 s was not obtained. The nature of these data and the environment suggested these arrivals could be accounted for by adding stochastic sound speed effects to the sound speed section (Colosi, 2016; Dushaw et al., 2016; Van Uffelen et al., 2010).

5. Internal Waves and Mediterranean Spice

The observed acoustic scattering that characterizes the overture is a general feature of acoustic arrival patterns obtained elsewhere, although it has been most often associated with the finale of midlatitude arrival patterns (Colosi, 2016; Colosi et al., 2005; Worcester et al., 1999). Two phenomena have been employed to account for

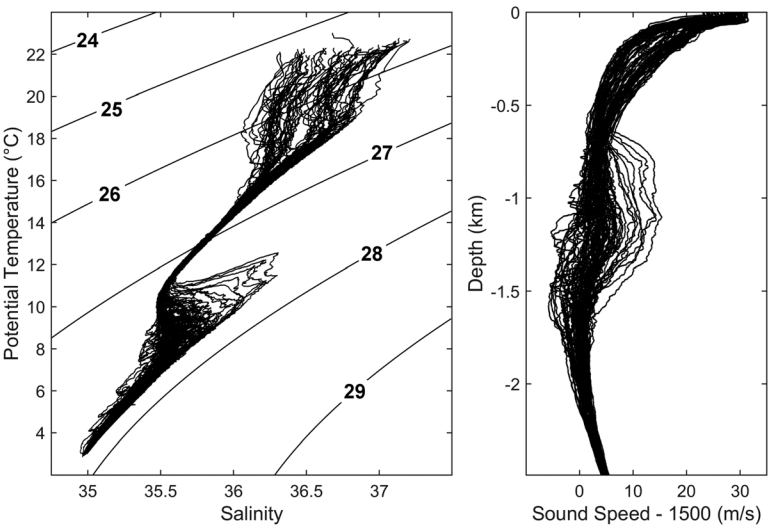

Figure 10. (left) *T–S* diagrams for 80 CTD casts and obtained during the deployment cruise for CAMBIOS in the Canary Basin (Figure 5). Values are for depths between the surface and 2.5 km. Contour values for sigma-*t* are shown to illustrate the variations of temperature and salinity along isopycnals. (right) Sound speed profiles associated with those casts. The significant influences of the spice of Mediterranean water on sound speed are obvious.

acoustically scattered signals like these. First, the sound speed fluctuations of internal waves are responsible for many scattering effects. Second, it is evident that the effects of spice, or the density-compensating fluctuations in temperature and salinity, are unavoidable, given obvious influence of Mediterranean water near the sound channel axis in this region (Figure 10). These two effects will be considered in turn.

5.1. Internal Waves

Stochastic models have been employed for the purposes of computing the effects of internal waves on acoustic propagation, e.g., Worcester et al. (1999), Colosi et al. (2005), Van Uffelen et al. (2010). While never a precise description of internal waves actually in the ocean, such models have been established as tools for addressing the issues of internal-wave effects on long-range acoustic propagation. We employed the internal-wave model of Colosi and Brown (1998) to construct a model for internal waves along the T1–T2 acoustic path using the climatological profiles for buoyancy, temperature and sound speed, and a latitude of 33°N (Figure 11, top). The parameters used for the model were a thermocline depth $B = 1{,}000$ m, spectrum indices $j_{max} = 100$ and $j_* = 3$, and ${\zeta_0}^2 = 32$, appropriate for a normal Garrett-Munk internal wave spectrum. N_0, the reference buoyancy, was computed as the buoyancy averaged over the upper 1,000 m, the depth of a nominal thermocline, giving a value 0.0080 rad s^{-1} (4.6 cy h^{-1}). For this internal wave strength, the sound speed variations near the sound channel axis are fairly small at 0.15 m s^{-1}. These fluctuations increase to 0.4 m s^{-1} just below the sound channel axis, corresponding to the base of Mediterranean water.

The effect of internal waves on the acoustic arrival pattern is to induce scattering along the branches of the timefront (Figure 9). The timefront is extended earlier, with the formation of several new arrivals between 205 and 205.5 s. The overture pattern is complicated and somewhat stochastic, however, much like the finale in comparable arrivals studied in the North Pacific, e.g., Colosi et al. (2005). The internal wave scattering induces the acoustic energy to extend to shallower depths, thus causing the predicted overture to look like the observed overture. In addition, the latest arriving branch of the timefront is extended later still, thus suggesting the final observed ray arrival (ray 9 in Figure 9). Both of these effects are manifestations of "shadow-zone arrivals" (Dushaw et al., 1999; Van Uffelen et al., 2010), that is, acoustic energy that arrives at depths where none is expected from computations using a smooth sound speed section. Note that the internal wave scattered overture exhibits a distinct arrival pattern of what look like stable rays. Similar patterns are evident in the observations at the beginning and ending of the record (Figure 3), but internal waves do not seem to account for the broad, stochastic nature of the overture that was most often observed.

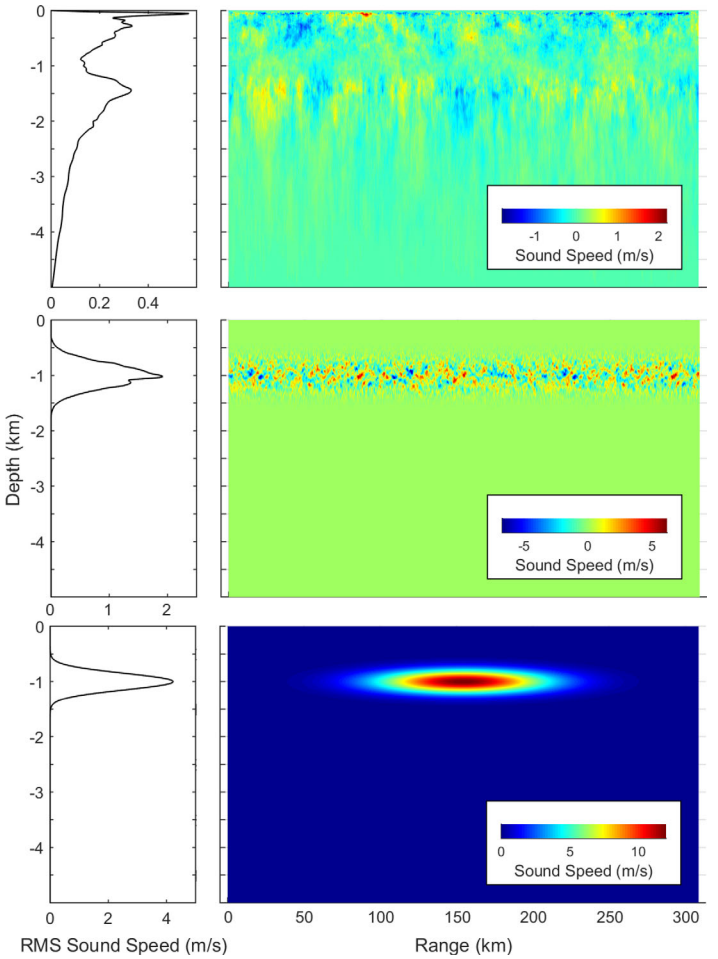

Figure 11. Three nominal perturbations to background sound speed environment. (left) The RMS sound speed as a function of depth of the right figures. (top) The Colosi-Brown internal-wave model for sound speed fluctuations derived from climatological temperature and bouyancy, and assuming a unit Garrett-Munk internal wave strength. The relatively large internal wave variations at about 1,500 m depth are due to greater temperature gradients at that depth (Figure 6). (middle) A model for the stochastic variations in sound speed arising from the spice of Mediterranean water near the sound channel axis. (bottom) An idealized Meddy with nominal spatial scales and nominal sound speed signature.

5.2. Stochastic Mediterranean Water

In the CTD and moored thermistor data obtained during CAMBIOS (Figures 7, 8, and 10), as well as the body of published evidence documenting Meddies, there is considerable evidence that parcels of Mediterranean water litter the ocean around the sound channel axis (the word "litter" is used here to suggest a sparse, stochastic distribution). The scales and other characteristics of Meddies and associated Mediterranean water are explicitly illustrated by the cross-sectional images that have been obtained by seismic methods (Biescas et al., 2008, 2014; Papenberg et al., 2010; Pinheiro et al., 2010; Quentel et al., 2011; e.g., Figure 12). In addition to Meddies, Mediterranean water can appear as a variety of different structures, such as submesoscale features, cyclones, and filaments (Quentel et al., 2011). The Meddy observed at mooring T3 (Figure 8) is consistent with the previous observations in showing a significant amount of such litter surrounding the Meddy. Temperature and salinity variations are evident in advance of, and trailing behind, the Meddy. Variations in temperature, salinity, and current stemmed from the Meddy and persisted for 30–40 days after its passage. As noted in the introduction, while this water has little variation in density, its sound speed variations are significant. The Colosi-Brown internal-wave model does not account for such spice variations, so an additional model is needed to accurately describe the acoustic environment.

The simple mesoscale model of Dushaw et al. (2016) was adapted for this purpose. This model was developed to account for the ubiquitous small-scale variability in Fram Strait. To qualitatively model the variations of Mediterranean water, the assumed covariance was centered on the sound channel axis, with variability decaying within several hundred meters away from the axis in depth. The vertical covariance was assumed to have the form

$$C(z1,z2)=3e^{\left(\frac{-(sz/2-1000)^2}{2\cdot 150^2}\right)}e^{\left(\frac{-dz^2}{sz}\right)}, \quad (1)$$

where $sz=z1+z2$ and $dz=z1-z2$. The variability in the vertical was modeled using the first 50 empirical orthogonal functions computed from this form; the variations of these functions with depth determine the scales of variability in the vertical. The horizontal variability was modeled using a truncated Fourier series with wavenumbers

$$K_n=\frac{2\pi n}{1.5R}, \quad (2)$$

where R is the path length, and the index n runs from 1 to 1,500. With this set of wavenumbers, the ad hoc wavenumber spectrum for the kth vertical mode was

$$S_k(K)=\frac{1}{K_{10k+20}^2+K^2}, \quad (3)$$

where the first term in the denominator ensures that higher-order vertical modes correspond to a whiter spectrum. With the vertical modes determined as above and with random amplitudes, chosen in accordance with the spectrum as above, applied to sines and cosines with wavenumbers as above, realizations for sound speed variations along the axis were readily computed (Figure 11, middle). The amplitude of the variations, determined by the leading value of the vertical covariance, was tuned to roughly correspond to the observed variations, such as those apparent in CTD casts (Figure 10, right). These variations were an order of magnitude larger than those of the internal waves, but confined near the sound channel axis.

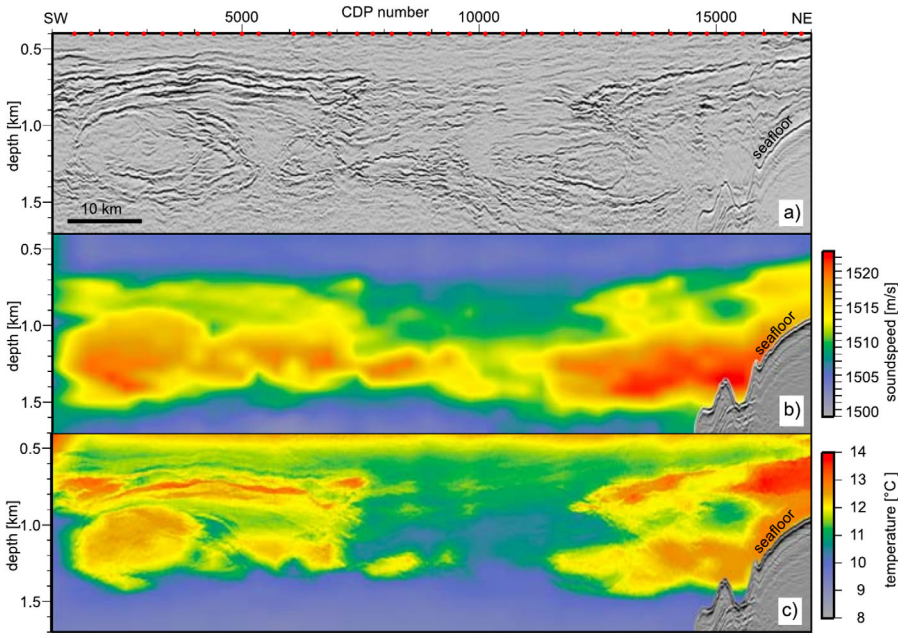

Figure 12. (a) Seismic and (b) hydrographic observations of a Meddy and other variability in the Eastern Atlantic near the Mediterranean outflow were combined by Papenberg et al. (2010) to obtained (c) estimates of temperature to fine scale. "CDP" refers to "Common Depth Points" of the seismic survey; seismic data are used to obtain cross-sectional estimates of structure at these points. The seismic measurements are mainly sensitive to sound speed contrasts. The range scale is indicated in the lower left corner of the top figure. The total section range is about 100 km. From Papenberg et al. (2010) by permission.

There were three general effects of this simulated stochastic Mediterranean water on the acoustic timefront. First, the overture energy was scattered more than from the internal wave variability. The nature of the timefront under the influence of this simulated variability was consistent with the observations. Second, the terminating branches of the timefront were extended later, considerably further than from internal wave scattering. The branch of the timefront that crosses the receiver depth at about 207.25 s is consistent with the observed ray arrival at about that time (ray arrival 9 in Figure 9). This last arrival is evidently a bottom-reflected, shadow-zone arrival. Lastly, the branches of the timefront are noticeably widened, indicating the scattering has increased noise in the travel times. The comparisons between the internal-wave and Mediterranean-water effects and the observations suggest that the latter has the dominant influence on acoustic propagation in this region.

6. A Simple Meddy Model

The common characteristics of Meddies are well documented. The observations of Meddies by CTD casts (Figures 6 and 10) and the T3 mooring (Figure 8) are consistent with these characterizations. The Meddy observed at the T3 mooring appears to have been relatively strong. To estimate the nominal effect a Meddy may have on acoustic travel times, a simple Gaussian-shaped sound speed perturbation was computed (Figure 11, bottom), based on common Meddy characteristics. This perturbation was added to the WOA09 sound speeds. Gaussian forms were employed

$$V(z) = e^{\frac{-(z-1000)^2}{2 \cdot 150^2}} \tag{4}$$

in depth and

$$H(r) = e^{\frac{-(R/2-r)^2}{2 \cdot 40000^2}} \tag{5}$$

in range, where R is the path length. With these expressions, the simulated Meddy was centered on 1,000 m depth and midway along the acoustic path, and it had a nominal 350 m vertical extent and

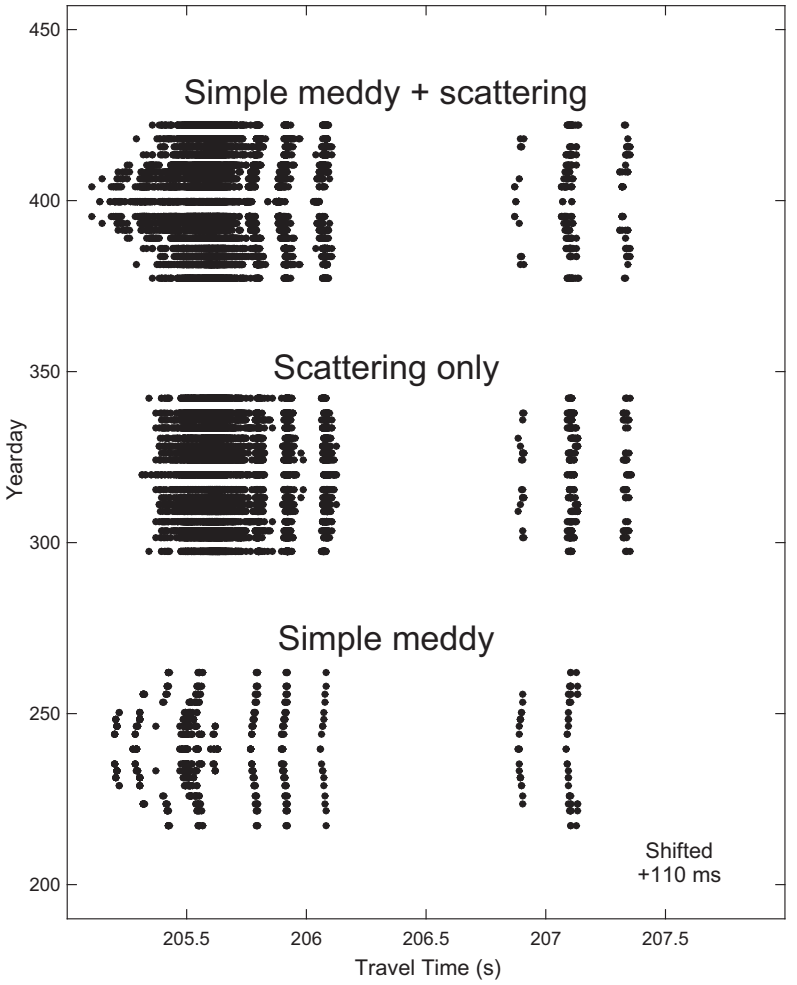

Figure 13. Three travel-time arrival patterns including influences of a simple Meddy model and acoustic scattering. The Meddy was Gaussian shaped with central sound speed 12 m s^{-1} greater than ambient. The lower pattern was computed using the simple simulated Meddy. The middle pattern was computed using only the addition of internal waves and spice variations. The upper pattern was computed using both of those models. The Meddy was assumed to move across the acoustic path at a rate of 4 cm s^{-1}. Rays that travel nearest the sound channel axis have the greatest deviation but are also greatly affected by acoustic scattering. Deep-turning rays are slightly affected. With scattering, an additional ray arrival is obtained. All travel times were offset by −110 ms. Compare with Figure 3.

94 km horizontal extent (full width at half maximum). The maximum Meddy sound speed perturbation was assumed to be 12 m s^{-1}.

With this Meddy model, rays were computed using a series of amplitudes: 0.0, 0.5, 1, 2, 4, 6, 8, 10, and 12 m s^{-1}. Since a given amplitude corresponds to a particular distance from Meddy center, assuming the Meddy moved at a nominal speed of 4 cm s^{-1} (Richardson & Tychensky, 1998) allows a time to be associated with each amplitude value. The ray travel times associated with this simulation of the passage of a Meddy across the center of the T1–T2 acoustic path is given in Figure 13, lower pattern. While the sound speed perturbation is large at the Meddy center, overall the effect on ray travel times over 309 km range is small, though not insignificant. Travel time perturbations of steep rays were about 10 ms, while perturbations of near-axis rays were about 30 ms. Three examples of the acoustic timefront for different Meddy amplitudes are given in Figure 14. The most obvious effect of a Meddy is the creation of many new ray arrivals within the overture, formed by the influence of the near-axis sound speed perturbations on near-axis acoustic propagation. Travel time variations of the earliest arriving acoustic energy may be caused more by the appearance of new rays than by temperature changes.

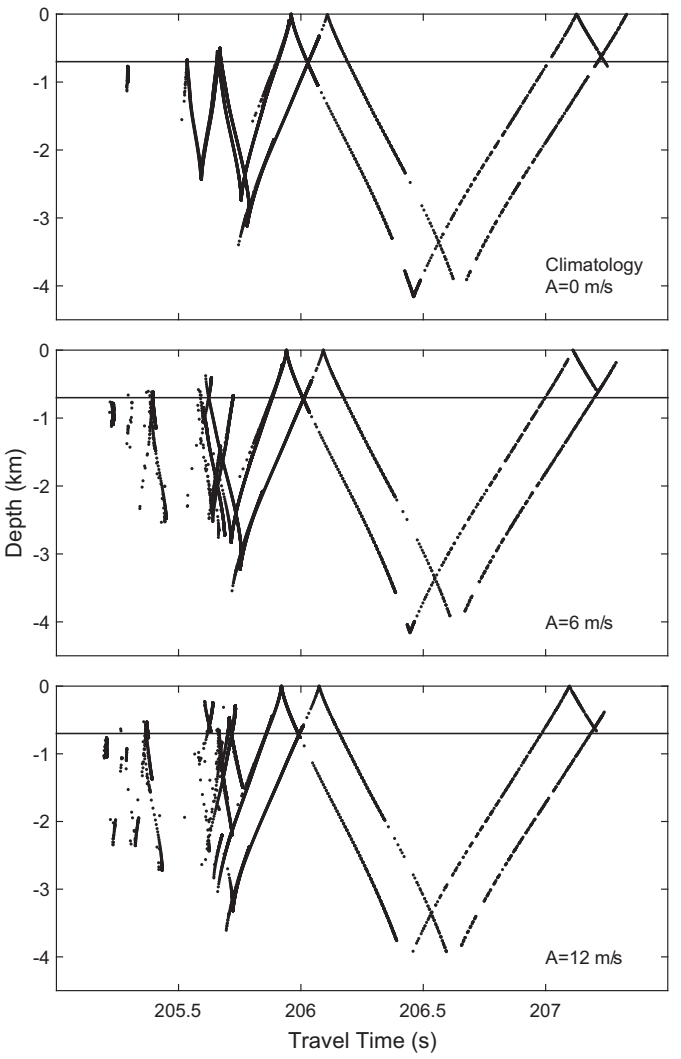

Figure 14. (top) Timefront for WOA09, as in Figure 9. (middle) Timefront for WOA09 plus a Meddy of 6 m s^{-1} maximum sound speed. (bottom) Timefront for WOA09 plus a Meddy of 12 m s^{-1} maximum sound speed. A Meddy along the acoustic path shifts the arrival pattern earlier and creates additional early arrivals.

The simulated Meddy had a dramatic effect on the ray paths. When the Meddy was at its maximum effect, the near-axis rays were split into two groups of rays traveling above and below the Meddy (Figure 15, middle). In effect, at Meddy maximum the dual sound channels became independently capable of supporting ray paths.

As has been described above, this simple model for a Meddy is entirely unrealistic, given the extraordinary variability from the Mediterranean water that surrounds Meddies. Combining the simple Meddy model with the stochastic and internal-wave models above, produces a sequence of arrival patterns (top pattern, Figure 13) that looks similar to the observations (Figure 3). Meddies evidently create additional ray paths, which are then thoroughly scattered by the small-scale sound speed fluctuations. This scattering significantly affects the ray paths as well (Figure 15), though such scattering preserves the integrity of the timefront for the deep-turning rays. The scattering also preserves the basic sampling characteristics of the deep-turning rays, that is, their upper and lower turning depths.

7. Horizontal Refraction

Meddies represent a large horizontal gradient in sound speed, hence may potentially be causing horizontal refraction of the tomographic signals (Voronovich et al., 2005). Such effects can be readily assessed by first computing the field of acoustic mode phase speed associated with a Meddy, and then computing the horizontal refraction of acoustic modes (Dushaw, 2014). The increased phase speed associated with Meddies serves to refract acoustic paths away from the Meddy. Such phase speeds were computed using the acoustic mode code KRAKEN (Jensen et al., 1994) and WOA09 climatological sound speed for the CAMBIOS region. The Meddy perturbation was that given by the example above, 12 m s^{-1} maximum sound speed, and the acoustic frequency was 400 Hz. The lowest acoustic modes were centered on the lower sound speed minimum at about 1,700 m, and they were unaffected by the presence of the Meddy at 1,000 m. Modes began to be affected by the Meddy when their vertical extent spanned Meddy depths. The largest effects were on mode numbers greater than about 40, which experienced a phase speed increase of about 2 m s^{-1}. The computed horizontal deflection of eigenrays experienced by such changes is less than about 50 m. Given the prevalence of acoustic scattering associated with propagation in this region, such horizontal refraction appears to be of no practical consequence.

8. Barotropic and Baroclinic Tides

Tidal variability offers an interesting test of the integrity of the acoustic data on the one hand, while also offering a test of the accuracy of tidal models. Global models for the barotropic tidal current (Stammer et al., 2014), which affects differential travel times, and mode-1 baroclinic tidal displacement (Dushaw, 2015; Dushaw et al., 2011), which affects sum travel times, are available. Both the differential and sum travel times were high-pass filtered with a 2 day running mean to better examine the tidal variability.

Unfortunately, the acoustic path was along the minor axis of the tidal currents for which the currents are weak (Figure 1), hence the barotropic tidal signal was expected to be small. Tidal models can accurately predict the acoustic barotropic tidal signal (and vice versa; Stammer et al., 2014). The TPXO model from Oregon State (Egbert & Erofeeva, 2002; Stammer et al., 2014) predicts peak-to-peak variations of only about 3 ms for the acoustic travel times for the T1–T2 acoustic path (Figure 16). For this experiment, the differential travel

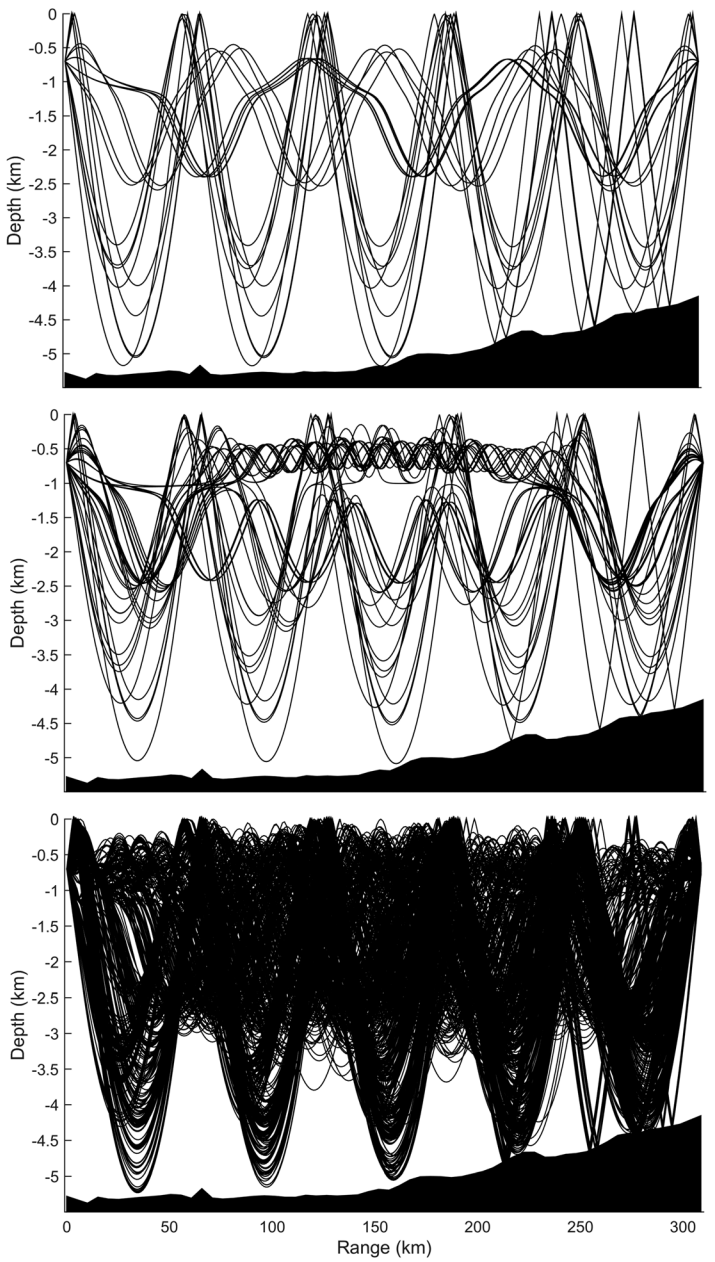

Figure 15. (top) Unperturbed ray paths, (middle) ray paths with hypothetical Meddy, and (bottom) ray paths with stochastic spice from Mediterranean water. A single sound speed section is used to compute the rays for each figure.

times were particularly noisy. Contributing factors include weak acoustic source level, inability to separate upward from downward propagating rays in the arrival pattern, the 20 min difference between reciprocal transmission times allowing for only partial cancellation of internal wave contributions (Dushaw et al., 1995), and the extraordinary acoustic scattering from Mediterranean water along the sound channel axis. As is evident in the differential travel times, the measurement noise is about an order of magnitude larger than the expected tidal variation.

Mode-1 baroclinic internal tides contribute a tidal variation to acoustic travel times, and, at least in the open ocean, these variations can be predicted (Dushaw, 2006, 2015; Dushaw et al., 1995, 2011). Zaron and Ray (2017) have used such predictions to partly remove tidal signals in hydrographic profile and surface current data. The signals from the baroclinic tides in acoustic travel times are caused by vertical displacements and their influence on sound speed. The variations of the sum of reciprocal travel times derived from CAMBIOS data can be used to test the internal tide predictability in the Canary Basin. An empirical global model for mode-1 internal tides recently derived from satellite altimetry data shows that the internal tides of the Canary Basin are a complicated interference of several wavetrains traveling in different directions (Figure 17; Dushaw, 2015). The model includes M_2, S_2, N_2, K_2, O_1, and K_1 tidal frequencies, although the altimetry data appear to only allow for resolution of the M_2 frequency and partial resolution of the S_2, O_1, and K_1 frequencies. The model appears to be the only one in existence that is capable of predicting the tidal variations in acoustic travel times from internal tides. In the comparisons below, note that altimetry data from 2000 to 2007 were used to predict travel time variations caused by internal waves in 1997–1998.

The internal tide models derived from satellite altimetry data are models for sea-surface height, so a sequence of computations is required to determine the associated travel time variations. First, the stratification is used to determine the internal wave modes, thus establishing the conversion from sea-surface height to internal displacement. The hydrographic conditions applied to the mode displacements then determine the sound speed variations. Lastly, the acoustic ray sampling determines the travel time variations associated with the sound speed variations (Dushaw, 2006; Dushaw et al., 1995, 2011). These computations were done using both the WOA09 climatology and the hydrographic data acquired along the acoustic path (Figure 7), but there was little difference between in the two estimated travel time variations.

The comparison between the observations and predictions over a 30 day section of data is shown in Figure 16, top. The sum travel times suffered the same noise problems as the differential travel times, but the tidal signal is evident. Note that by historical precedence, the sum travel times are the average of reciprocal travel times while the differential travel times are just the difference. The two variables therefore differ in scale by a factor of 2. The predicted and observed internal tide variations agreed in phase, but the observed amplitudes varied irregularly and were larger than predicted. A clearer comparison can be made by comparing estimates of mode-1 amplitude derived from the travel times to equivalent mode amplitude derived from the altimetric model (Figure 18). A simple inverse employing baroclinic sound speed modes as vertical basis functions was employed for this purpose (Dushaw, 2006; Dushaw et al., 1995). These modes were derived from the CAMBIOS hydrographic data obtained along the acoustic path. While the data suffered

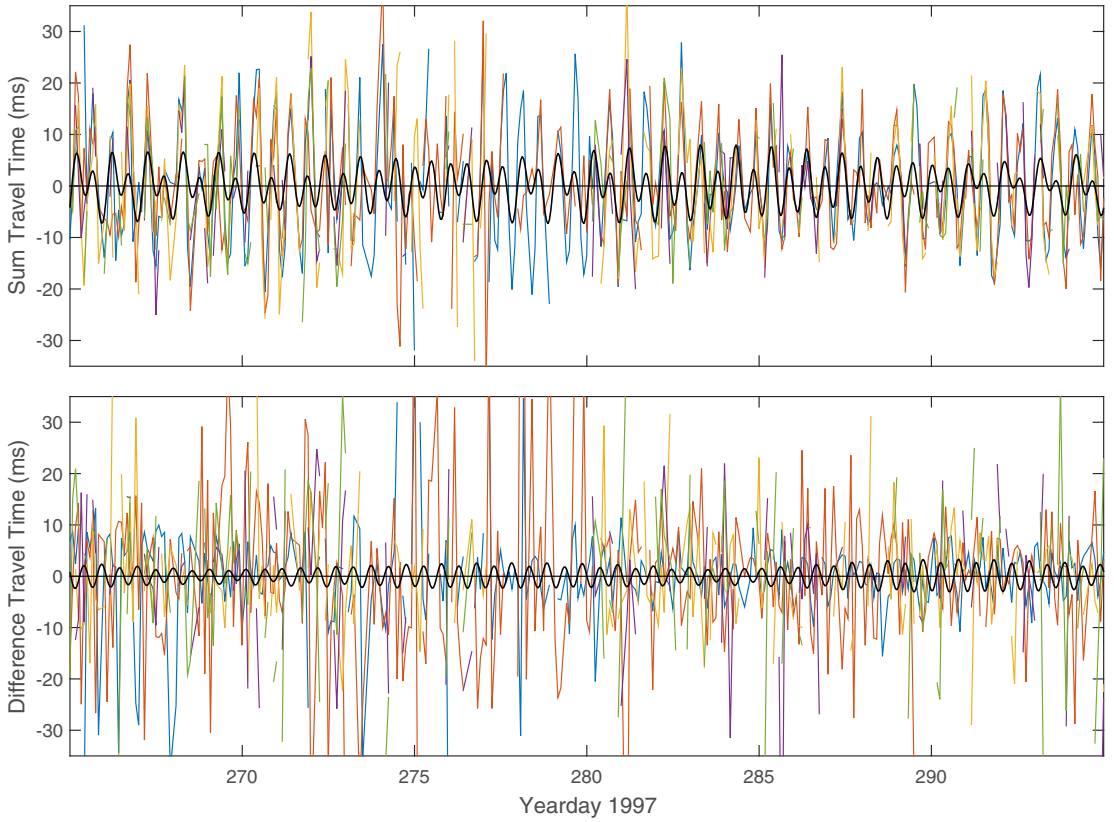

Figure 16. Thirty days of high-frequency (>0.5 cpd) for (top) sum travel times and (bottom) difference travel times. Only travel times for ray arrivals 3, 4, 6, 7, and 8 are shown, which have the clearest signal. The sum travel times exhibit the obvious signal of mode-1 internal tides which compares favorably to an independent prediction for them (black line). The differential travel times are too noisy to resolve the tidal current variations, as evident from the comparison to the tidal prediction derived from the TPXO v.8 global tidal model (black line). Note that the sum travel times are the average of reciprocal travel times, while differential travel times are simply the difference.

from considerable noise, as noted above, it is also apparent that there were considerable irregular variations in the tidal amplitude. A tidal analysis of the 275 day time series of estimated mode-1 amplitude was computed by a least squares fit using the frequencies of the eight largest tidal constituents. The tidal fit accounted for only 19% of the variance. Similar acoustic observations in the Pacific or Atlantic (Dushaw, 2006; Dushaw et al., 1995, 2011) observed more coherent internal tides. In those observations, tidal analyses accounted for 40–70% of the variance. The internal tide variations observed in the Pacific and Atlantic experiments had temporal coherence that was similar to the coherence of tidal variations from the barotropic currents observed in those experiments. Evidently, the Canary Basin the mode-1 internal tides are not as phase locked, or have greater variations in amplitude, than has been observed elsewhere. Nevertheless, the altimetric model predictions compare favorably to the coherent component of the internal tide, as estimated by the results of the tidal analysis of the acoustic time series (Figure 18). The comparisons in other sections of the record length are similar. Under the circumstances, the agreement between the independent predictions and observations is remarkable.

9. Discussion

As a test of the ability of ocean acoustic tomography to measure the properties and fluxes of Mediterranean water through the Canary Basin, the CAMBIOS acoustical observations give an ambiguous result at present. On the one hand, some deficiencies in the observations, particularly the inability to distinguish upward from downward traveling rays, prevented the derivation of an optimal timeseries. On the other hand, while Meddies provide a significant influence on the acoustic propagation, it was difficult to distinguish their effects from those of the stochastic parcels of Mediterranean water that appear to litter the sound channel

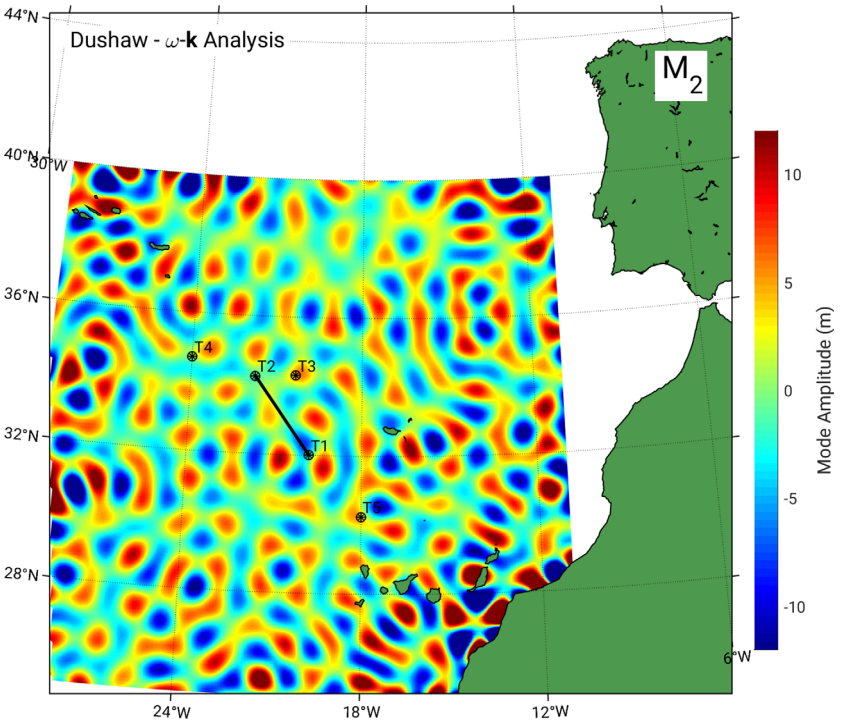

Figure 17. A snapshot of mode-1, M_2 internal tides for the CAMBIOS region derived from the empirical model of Dushaw (2015). The internal tide field is a complicated interference pattern. The black segment indicates the T1–T2 acoustic path.

of the Canary Basin. It is all but certain that at least one Meddy crossed the acoustic path; the Meddy recorded at the T3 mooring was strong and consistent with the southwestward movement of Meddies that has been commonly reported. Figure 19 shows the Meddy temperature timeseries recorded at T3, shifted by 25 days to roughly account for the time it would have taken the Meddy to reach the T1–T2 acoustic path, next to the acoustical observations. While the extended duration of the overture section of the arrival pattern is consistent with the simple Meddy model and stochastic effects as modeled above, the lingering of that signal over 80 or more days does not appear to be consistent with general patterns of Meddy motion. That the Meddy may have stalled, or another Meddy arrived, are equal possibilities, however. It is not readily apparent how an inverse of the overture portion of travel time data for estimation of ocean properties can be accomplished, given the extraordinary nonlinearity of the situation.

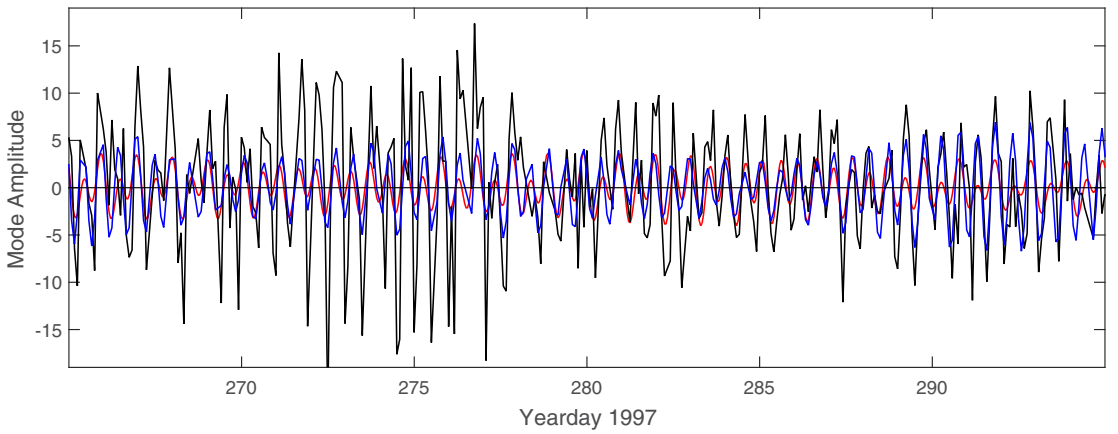

Figure 18. Time series of internal tide mode-1 amplitude estimated from an inverse of travel times (black) and a tidal analysis of that time series (blue). The amplitude is unitless, but the mode normalization is such that mode amplitude is about equal to vertical displacement in meters at mode maximum. An independent prediction for the tidal time series was derived from satelite alitmetry (red). While the data are noisy, it is also evident that considerable in situ internal tide variability is not phase locked, hence not predictable.

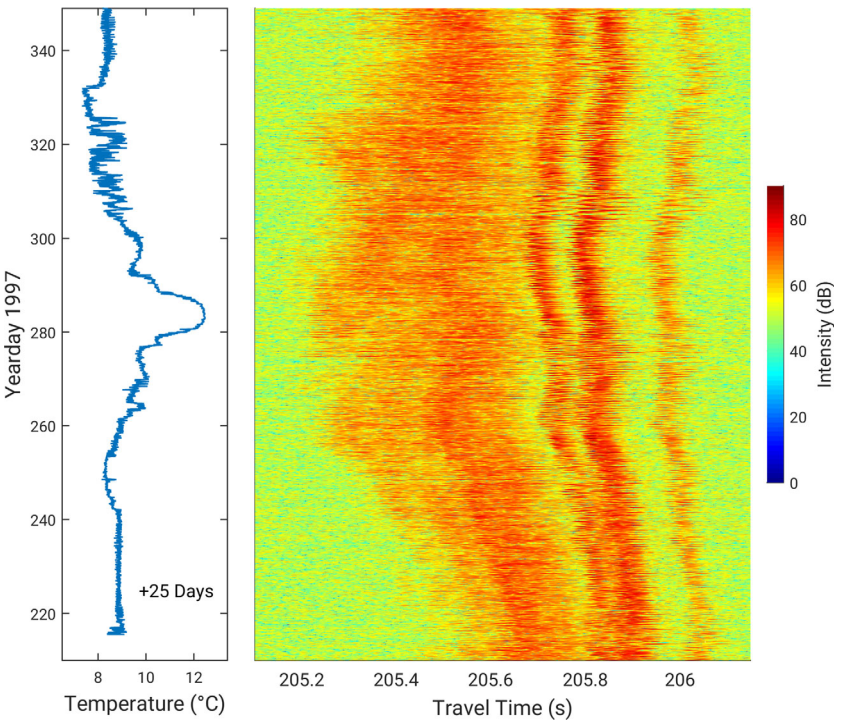

Figure 19. Close-up view of the measured acoustic travel time patterns during (right) the time of expected Meddy influences, compared to (left) the time variation of temperature observed on mooring T3. The latter time series was delayed by 25 days, roughly the length of time it would take a Meddy to travel from the mooring to the acoustic path.

Ideally, the acoustic tomography measurements would be combined with all available measurements through ocean modeling and data assimilation (Gaillard, 1992; Rémy et al., 2002). The data used for this purpose would necessarily be the simple travel times of the identified, deep-turning rays. Such modeling puts the acoustic measurements in a larger dynamical context, hence it highlights the essential meaning of the observations. The complicated recorded travel times associated with the initial portion of the arrival pattern are a measurement of the large scale temperature variations associated with Mediterranean water along the sound channel axis. Some of the variations may be Meddies, others may be more complicated manifestations of Meditarranean water. As a practical matter, the dominance of acoustic scattering effects precludes the acoustical measurement of the small signals of Meddy currents or relative vorticity. (The 20 cm s^{-1} current speeds within Meddies would produce travel time variations of a mere fraction of a millisecond.) In

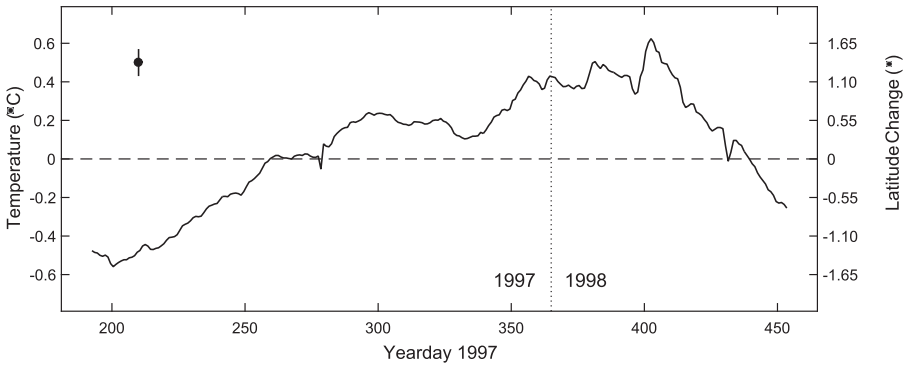

Figure 20. Temperature relative to the time-mean temperature estimated from the identified-ray travel times. The estimated temperature is an average over the range of the path and over 0–2,000 m depth interval. The formal inverse uncertainty is about 0.07°C as indicated at top left. The temperature variations can be mostly accounted for by latitudinal variations in the Azores Current. The scale at right indicates the approximate equivalent changes in latitude.

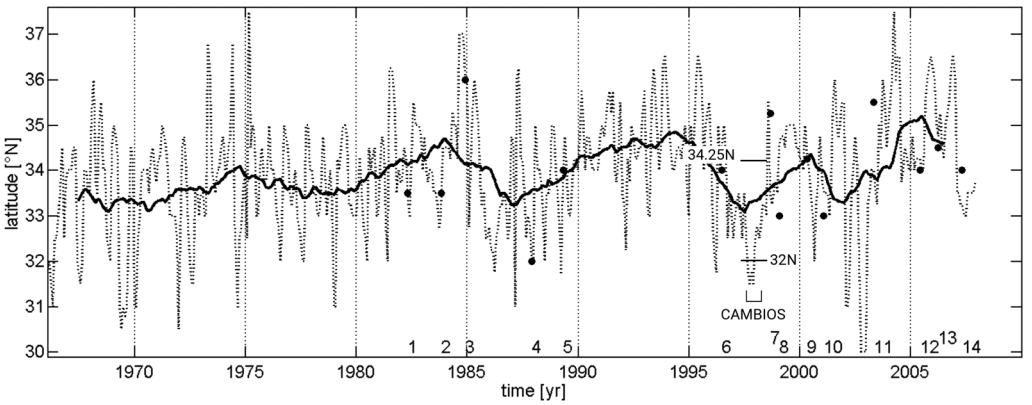

Figure 21. The estimated latitude of the Azores Current at 22°W between 1965 and 2008 derived from SODA POP state estimates. The solid line is a 3 year running mean. The latitude range of the CAMBIOS tomography path is indicated; this path was between 19.8°W and 21.75°W longitude. Over the observation time period of CAMBIOS, latitudinal variations of 1°–2° were estimated. The black dots denote independent estimates of Current position derived from in situ measurement. From Fründt and Waniek (2012) by Creative Commons License and permission of the authors.

seems apparent that these measurements indicate the persistent southwestward flux of temperature and salt by the movement of Mediterranean water, generally.

Barotropic tidal currents were not detected in the tomography data acquired during CAMBIOS, both because of the small signal expected and the considerable noise in the differential travel times obtained. Internal tide signals were measured, though a tidal analysis of the time series of mode-1 amplitude estimated from the travel times accounted for only 20% of the variance. The coherent tidal variability estimated from that tidal analysis was predicted reasonably well by an independent empirical global model derived from satellite altimetry. This variability accounts for only a small portion of the tides in this case, however. While some agreement was anticipated, given the several other similar comparisons obtained worldwide (Dushaw, 2015; Dushaw et al., 2011), the result suggests that the Canary Basin may be one region where these tides are not particularly predictable.

The later-arriving, resolved-ray travel times varied by about 300 ms over the course of the experiment. This variability was roughly consistent with an annual cycle, but maximum temperatures (least travel times) were obtained in January 1998. Further, the variation was observed by all rays, even those that turn below 500 m depth, hence the variation was not caused by heat flux at the surface. Such changes can be readily accounted for by latitudinal movement of the Azores Current. A simple inverse employing objective mapping techniques was applied to the resolved-ray travel times to estimate average ocean temperature (Figure 20; Cornuelle et al., 1993). Such estimates were for temperature variations relative to the time mean. The inverse employed baroclinic modes in the vertical and a truncated Fourier series in the horizontal. The solution was averaged over range and over 0–2,000 m depth. Estimated uncertainties for this average temperature and ocean model were ± 0.067°C. The uncertainty of a full-depth average was an order of magnitude smaller. Relative to the time-mean temperature, the temperature averaged over the CAMBIOS tomography path varied from about -0.5°C at the start of the experiment to about $+0.4$°C during January and February 1998, before cooling again to about -0.2°C by the end of the experiment. Such variations can be mostly accounted for by latitudinal motions of the Azores Current. From the CTD data obtained during CAMBIOS, the 0–2,000 m average temperature change across the Current is 0.7°C. A movement of the Current over the latitude range of the CAMBIOS moorings therefore would correspond to this temperature change, which sets the scaling factor between observed temperature and latitude change. Relative to mean, the temperature variations corresponded to latitudinal variations from about $-1.1°$ at the start of the experiment to $+1.1°$ in winter 1998. Such shifts in Current latitude are well within the monthy variations obtained from numerical ocean state estimates determined by the Simple Ocean Data Assimilation Parallel Ocean Program (SODA POP; Fründt & Waniek, 2012; Figure 21). Ultimately, the origins of the observed interannual temperature variation cannot be determined by the present analysis, however. Thermistors at 1,200 m depth on the T1 and T2 moorings did not record much change in temperature at all (not shown), hence, at the very least, the Azores Current did not move over the tomography moorings.

The presence of the Azores Current lends an interesting possible factor to the interpretations of the Meddy and the internal tide signals in acoustic travel time. As noted by Bashmachnikov et al. (2015), fewer Meddies are found south of the Current, indicating a substantial Meddy-Current interaction. As stated by Bashmachnikov et al. (2015), the Current acts as a dynamic barrier for Meddies. It is possible the nature of the observed travel time data, that is, the extended effects of small-scale variability over the record length, was a consequence of the interaction of the T3 Meddy with the Azores Current. The Azores Current may also have acted to diminish the coherence of the internal tide. Previous observations of internal tides by tomography showed more temporal coherence, but those observations were made in areas well away from current systems.

Acknowledgments

B. Dushaw was supported by ONR grant N00014–15-1–2186 and NASA grant NNX13AE27G. This work is a contributrion to the CAMBIOS integrated project which was financed by the European Union in the 6th Framework Programme for Research and Development. F. Gaillard, T. Terre, and the CAMBIOS experiment were supported by the MAST III CANIGO programme (contract MAS3-CT96-0060). We also acknowledge the efficient, professional support for the deployment, and recovery of the moorings, and for the hydrographic surveys, provided by the crew of the N/O Thalassa operated by IFREMER. The data supporting the conclusions of this analysis can be obtained through the cited references and their associated web links. The direct link to the CAMBIOS data set is http://campagnes.flotteoceanographique.fr/series/230/.

References

Antonov, J. I., Seidov, D., Boyer, T. P., Locarnini, R. A., Mishonov, A. V., Garcia, H. E., . . . Johnson, D. R. (2010). World Ocean Atlas 2009. Volume 2: Salinity. In S. Levitus (Ed.), *NOAA Atlas NESDIS 69* (184 pp.). Washington, DC: United States Government Printing Office.

Armi, L., & Zenk, W. (1984). Large lenses of highly saline Mediterranean water. *Journal of Physical Oceanography*, *14*, 1560–1576. https://doi.org/10.1175/1520-0485(1984)014<1560:LLOHSM>2.0.CO;2

Bashmachnikov, I., Machín, F., Mendonça, A., & Martins, A. (2009). In situ and remote sensing signature of Meddies east of the mid-Atlantic ridge. *Journal of Geophysical Research*, *114*, C05018. https://doi.org/10.1029/2008JC005032

Bashmachnikov, I., Neves, F., Calheiros, T., & Carton, X. (2015). Properties and pathways of Mediterranean water eddies in the Atlantic. *Progress in Oceanography*, *137*, 149–172. https://doi.org/10.1016/j.pocean.2015.06.001

Biescas, B., Ruddick, B. R., Nedimovic, M. R., Sallarès, V., Bornstein, G., & Mojica, J. F. (2014). Recovery of temperature, salinity, and potential density from ocean reflectivity. *Journal of Geophysical Research: Oceans*, *119*, 3171–3184. https://doi.org/10.1002/2013JC009662

Biescas, B., Sallarès, V., Pelegrí, J. L., Machín, F., Carbonell, R., Buffett, G., . . . Calahorrano, A. (2008). Imaging meddy finestructure using multichannel seismic reflection data. *Geophysical Research Letters*, *35*, L11609. https://doi.org/10.1029/2008GL033971

Colosi, J. (2016). *Sound propagation through the stochastic ocean* (424 pp.). Cambridge, UK: Cambridge University Press.

Colosi, J. A., Baggeroer, A. B., Cornuelle, B. D., Dzieciuch, M. A., Munk, W. H., Worcester, P. F., . . . Forbes, A. M. G. (2005). Analysis of multipath acoustic field variability and coherence in the finale of broadband basin-scale transmissions in the North Pacific Ocean. *Journal of the Acoustical Society of America*, *117*, 1538–1564. https://doi.org/10.1121/1.1854615

Colosi, J. A., & Brown, M. G. (1998). Efficient numerical simulation of stochastic internal-wave-induced sound-speed perturbation fields. *Journal of the Acoustical Society of America*, *103*, 2232–2235. https://doi.org/10.1121/1.421381

Cornuelle, B., Worcester, P. F., Hildebrand, J. A., Hodgkiss, W. S., Jr., Duda, T. F., Boyd, J., . . . Spindel, R. C. (1993). Ocean acoustic tomography at 1000-km range using wavefronts measured with a large-aperture vertical array. *Journal of Geophysical Research*, *98*, 16365–16377. https://doi.org/10.1029/93JC01246

Del Grosso, V. A. (1974). New equation for the speed of sound in natural waters (with comparisons to other equations). *Journal of the Acoustical Society of America*, *56*, 1084–1091.

Dushaw, B. D. (2006). Mode-1 internal tides in the western North Atlantic Ocean. *Deep Sea Research Part I: Oceanographic Research Papers*, *53*, 449–473. https://doi.org/10.1016/j.dsr.2005.12.009

Dushaw, B. D. (2014). Assessing the horizontal refraction of ocean acoustic tomography signals using high-resolution ocean state estimates. *Journal of the Acoustical Society of America*, *136*, 122–129. https://doi.org/10.1121/1.4881928

Dushaw, B. D. (2015). *An empirical model for mode-1 internal tides derived from satellite altimetry: Computing accurate tidal predictions at arbitrary points over the world oceans* (Tech. Memo. TM 1–15, 114 pp.). Seattle, WA: Applied Physics Laboratory, University of Washington. Retrieved from http://www.apl.washington.edu/project/project.php?id=tm_1-15

Dushaw, B. D., & Colosi, J. A. (1998). *Ray tracing for ocean acoustic tomography* (APL-UW TM 3–98, 31 pp.). Seattle, WA: Applied Physics Laboratory, University of Washington.

Dushaw, B. D., Howe, B. M., Mercer, J. A., Spindel, R. C., Baggeroer, A. B., Menemenlis, D., . . . Munk, W. (1999). Multimegameter-range acoustic data obtained by bottom-mounted hydrophone arrays for measurement of ocean temperature. *IEEE Journal of Oceanic Engineering*, *24*, 202–214. https://doi.org/10.1109/48.757271

Dushaw, B. D., Menemenlis, D., Worcester, P. F., & Dzieciuch, M. A. (2013). On the time-mean state of ocean models and the properties of long range acoustic propagation. *Journal of Geophysical Research: Oceans*, *118*, 4346–4362. https://doi.org/10.1002/jgrc.20325

Dushaw, B. D., Sagen, H., & Beszczynska-Möller, A. (2016). On the effects of small-scale variability on acoustic propagation in Fram Strait: The tomography forward problem. *Journal of the Acoustical Society of America*, *140*, 1286–1299. https://doi.org/10.1121/1.4961207

Dushaw, B. D., Worcester, P. F., Cornuelle, B. D., Howe, B. M., & Luther, D. S. (1995). Baroclinic and barotropic tides in the central North Pacific Ocean determined from long-range reciprocal acoustic transmissions. *Journal of Physical Oceanography*, *25*, 631–647. https://doi.org/10.1175/1520-0485(1995)025<0631:BABTIT>2.0.CO;2

Dushaw, B. D., Worcester, P. F., & Dzieciuch, M. A. (2011). On the predictability of mode-1 internal tides. *Deep Sea Research Part I: Oceanographic Research Papers*, *58*, 677–698. https://doi.org/10.1016/j.dsr.2011.04.002

Egbert, G. D., & Erofeeva, S. Y. (2002). Efficient inverse modeling of barotropic ocean tides. *Journal of Atmospheric and Oceanic Technology*, *19*, 183–204. https://doi.org/10.1175/1520-0426(2002)019<0183:EIMOBO>2.0.CO;2

Fründt, B., & Waniek, J. J. (2012). Impact of the Azores Front propagation on deep ocean particle flux, *Central European Journal of Geosciences*, *4*, 531–544. https://doi.org/10.2478/s13533-012-0102-2

Gac, C., Le Gall, Y., & Terre, T. (1999). For ocean acoustic tomography new modular instrumentation. *Sea Technology*, *40*, 55–60.

Gac, C., Le Gall, Y., Terre, T., Leduc, B., & Person, R. (1998). A new modular instrumentation for ocean acoustic tomography, present status and future trends, In *IEEE OCEANS '98 Conference Proceedings* (Vol. 3, pp. 1219–1223). Retrieved from https://doi.org/10.1109/OCEANS.1998.726262

Gaillard, F. (1992). Evaluating the information content of tomographic data: Application to mesoscale observations. *Journal of Geophysical Research*, *97*, 15489–15505. https://doi.org/10.1029/92JC01295

Gaillard, F., Billant, A., & Branellec, P. (1998). *CAMBIOS—Volume 1: Campagne Cambios 97—Rapport de données CTD-O2* (Unité mixte 6523 (CNRS/IFREMER/UBO), R. INT. DRO/DOPS/LPO 98-02, 184 pp.). Direction des Recherches Océaniques, DRO/UM/LPO, Laboratoire de Physique des Océans. Retrieved from http://archimer.ifremer.fr/doc/00210/32140/

Gaillard, F., Billant, A., & Branellec, P. (1999a). *CAMBIOS—Volume 4: Campagne Cambios 98—Rapport de données CTD-O2—Contribution CANIGO (MAS3-CT96-0060)* (Unité mixte 6523 (CNRS/IFREMER/UBO), R. INT. DRO/DOPS/LPO 99-05, 159 pp.). Direction des Recherches Océaniques, DRO/UM/LPO, Laboratoire de Physique des Océans. Retrieved from http://archimer.ifremer.fr/doc/00233/34399/

Gaillard, F., Billant, A., & Branellec, P. (1999b). *CAMBIOS—Contribution à CANIGO (MAS3-CT96-0060)—Volume 2: Expérience CAMBIOS—Rapport des données eulériennes sur les 4 mouillages* (Unité mixte 6523 (CNRS/IFREMER/UBO), R. INT. DRO/DOPS/LPO 99-2, 118 pp.). Direction des Recherches Océaniques, DRO/UM/LPO, Laboratoire de Physique des Océans. Retrieved from http://archimer.ifremer.fr/doc/00233/34397/

Gaillard, F., Lherminier, P., Lagadec, C., & Branellec, P. (2015). *CAMBIOS, station profiles: CTD and LADCP*. SEANOE. https://doi.org/10.17882/40905

Gaillard, F., & Terre, T. (2003). *CAMBIOS contribution à CANIGO (MAS3-CT96-0060). Volume 7: Expérience CAMBIOS. Traitement des données de tomographie* (Unité mixte 6523 (CNRS/IFREMER/UBO), R. INT. DRO/DOPS/LPO 03–11, 141 pp.). Direction des Recherches Océaniques, DRO/UM/LPO, Laboratoire de Physique des Océans. Retrieved from http://archimer.ifremer.fr/doc/00312/42332/

Gaillard, F., & Terre, T. (2004). *CAMBIOS contribution CANIGO (MAS3-CT96-0060). Volume 8: Exprience CAMBIOS. Analyse des donnes de tomographie* (Unité mixte 6523 (CNRS/IFREMER/UBO), R. INT. DRO/DOPS/LPO 04-03, 45 pp.). Direction des Recherches Océaniques, DRO/UM/LPO, Laboratoire de Physique des Océans. Retrieved from http://archimer.ifremer.fr/doc/00312/42333/

Gaillard, F., Terre, T., & Guillot, A. (2006). Monitoring moored instrument motion by optimal estimation. *Ocean Engineering*, *33*, 1–22. https://doi.org/10.1016/j.oceaneng.2005.04.011

Ienna, F., Jo, Y. H., & Yan, X.-H. (2014). A new method for tracking Meddies by satellite altimetry. *Journal of Atmospheric and Oceanic Technology*, *31*, 1434–1445. https://doi.org/10.1175/JTECH-D-13-00080.1

Jensen, F. B., Kuperman, W. A., Porter, M. B., & Schmidt, H. (1994). *Computational ocean acoustics* (621 pp.). New York, NY: Springer.

Locarnini, R. A., Mishonov, A. V., Antonov, J. I., Boyer, T. P., Garcia, H. E., Baranova, O. K., . . . Johnson, D. R. (2010). World Ocean Atlas 2009, Volume 1: Temperature. In S. Levitus (Ed.), *NOAA Atlas NESDIS 68* (184 pp.). Washington, DC: United States Government Printing Office.

Menemenlis, D., Campin, J., Heimbach, P., Hill, C., Lee, T., Nguyen, A., . . . Zhang, H. (2008). ECCO2: High resolution global ocean and sea ice data synthesis. *Mercator Ocean Quarterly Newsletter*, *31*, 13–21.

Mikhin, D. Y., Godin, O. A., Boebel, O., & Zenk, W. (1997). Simulations of acoustic imprints of Meddies in the Iberian Basin: Toward detection of Meddies. *Journal of Atmospheric and Oceanic Technology*, *14*, 938–949. https://doi.org/10.1175/1520-0426(1997)014<0938:SOAIOM>2.0.CO;2

Munk, W., Worcester, P., & Wunsch, C. (1995). *Ocean acoustic tomography* (456 pp.). Cambridge, UK: Cambridge University Press.

Papenberg, C., Klaeschen, D., Krahmann, G., & Hobbs, R. W. (2010). Ocean temperature and salinity inverted from combined hydrographic and seismic data. *Geophysical Research Letters*, *37*, L04601. https://doi.org/10.1029/2009GL042115

Parrilla, G., Neuer, S., Le Traon, P.-Y., & Fernández-Suarez, E. (2002). Topical studies in oceanography: Canary Islands Azores Gibraltar Observations (CANIGO): Volume 1: Studies in the northern Canary Islands basin. *Deep Sea Research Part II: Topical Studies in Oceanography*, *49*, 3409–3413. https://doi.org/10.1016/S0967-0645(02)00104-2

Pinheiro, L. M., Song, H., Ruddick, B., Dubert, J., Ambar, I., Mustafa, K., & Bezerra, R. (2010). Detailed 2-D imaging of Mediterranean outflow and Meddies off W Iberia from multichannel seismic data. *Journal of Marine Systems*, *79*, 89–100. https://doi.org/10.1016/j.jmarsys.2009.07.004

Quentel, E., Carton, X., & Gutscher, M. A. (2011). Structure and temporal variability of Mediterranean water in hydrological and marine seismic data south of Portimao Canyon (Gulf of Cadiz), from 1999 to 2001. *International Journal of Geosciences*, *2*, 185–194. https://doi.org/10.4236/ijg.2011.23020

Rémy, E., Gaillard, F., & Verron, J. (2002). Variational assimilation of ocean tomographic data: Twin experiments in a quasi-geostrophic model. *Quarterly Journal of the Royal Meteorological Society*, *128*, 1739–1458. https://doi.org/10.1002/qj.200212858317

Richardson, P. L., Bower, A. S., & Zenk, W. (2000). A census of Meddies tracked by floats. *Progress in Oceanography*, *45*, 209–250. https://doi.org/10.1016/S0079-6611(99)00053-1

Richardson, P. L., & Tychensky, A. (1998). Meddy trajectories in the Canary Basin measured during the SEMAPHORE experiment, 1993–1995. *Journal of Geophysical Research*, *103*, 25029–25045. https://doi.org/10.1029/97JC02579

Send, U., Worcester, P. F., Cornuelle, B. D., Tiemann, C. O., & Baschek, B. (2002). Integral measurements of mass transport and heat content in the Strait of Gibraltar from acoustic transmissions. *Deep Sea Research Part II: Topical Studies in Oceanography*, *49*, 4069–4095. https://doi.org/10.1016/S0967-0645(02)00143-1

Smith, W. H. F., & Sandwell, D. T. (1997). Global seafloor topography from satellite altimetry and ship depth soundings. *Science*, *277*, 1957–1962.

Spindel, R. C., Worcester, P. F., Webb, D. C., Boutin, P. R., Peal, K. R., & Bradley, A. M. (1982). Instrumentation for ocean acoustic tomography. *Proceedings of the IEEE Conference Oceans*, *82*, 92–99. https://doi.org/10.1109/OCEANS.1982.1151739

Stammer, D., Hinrichsen, H., & Käse, R. H. (1991). Can Meddies be detected by satellite altimetry? *Journal of Geophysical Research*, *96*, 7005–7014.

Stammer, D., Ray, R. D., Andersen, O. B., Arbic, B. K., Bosch, W., Carrère, L., . . . Yi, Y. (2014). Accuracy assessment of global barotropic ocean tide models. *Reviews of Geophysics*, *52*, 243–282. https://doi.org/10.1002/2014RG000450

Terre, T., & Gaillard, F. (2003). *Expérience CAMBIOS Rapport des donnes de tomographie, Volume 6* (Unité mixte 6523 (CNRS/IFREMER/UBO), R. INT. DRO/DOPS/LPO 03-1, 94 pp.). Direction des Recherches Océaniques, DRO/UM/LPO, Laboratoire de Physique des Océans. Retrieved from http://archimer.ifremer.fr/doc/00312/42331/

Tiemann, C. O., Worcester, P. F., & Cornuelle, B. D. (2001). Acoustic remote sensing of internal solitary waves and internal tides in the Strait of Gibraltar. *Journal of the Acoustical Society of America*, *110*, 798–811. https://doi.org/10.1121/1.1382617

Van Uffelen, L. J., Worcester, P. F., Dzieciuch, M. A., Rudnick, D. L., & Colosi, J. A. (2010). Effects of upper ocean sound-speed structure on deep acoustic shadow-zone arrivals at 500- and 1000-km range. *Journal of the Acoustical Society of America*, *127*, 2169–2181. https://doi.org/10.1121/1.3292948

Voronovich, A. G., Ostashev, V. E., Colosi, J. A., Cornuelle, B. D., Dushaw, B. D., Dzieciuch, M. A., . . . The NPAL Group. (2005). Horizontal refraction of acoustic signals retrieved from North Pacific Acoustic Laboratory billboard array data. *Journal of the Acoustical Society of America*, *117*, 1527–1537. https://doi.org/10.1121/1.1854435

Voronovich, A. G., & Shang, E. C. (1999). Horizontal refraction modal tomography of the ocean with mode interactions. *IEEE Journal of Oceanic Engineering*, *24*, 224–231. https://doi.org/10.1109/48.757273

Worcester, P. F., Cornuelle, B. D., Dzieciuch, M. A., Munk, W. H., Howe, B. M., Mercer, J. A., . . . Baggeroer, A. B. (1999). A test of basin-scale acoustic thermometry using a large-aperture vertical array at 3250-km range in the eastern North Pacific Ocean. *Journal of the Acoustical Society of America*, *105*, 3185–3201.

Zaron, E. D., & Ray, R. (2017). Using an altimeter-derived internal tide model to remove tides from in situ data. *Geophysical Research Letters*, *44*, 4241–4245. https://doi.org/10.1002/2017GL072950